REVIEW

Geometry of the Meridional Overturning Circulation at the Last Glacial Maximum

FRANK J. PAVIA,[a] C. SPENCER JONES,[b,c] AND SOPHIA K. HINES[d]

[a] Department of Geological and Planetary Sciences, Caltech, Pasadena, California
[b] Texas A&M University, College Station, Texas
[c] Lamont-Doherty Earth Observatory of Columbia University, Palisades, New York
[d] Department of Marine Chemistry and Geochemistry, Woods Hole Oceanographic Institution, Woods Hole, Massachusetts

(Manuscript received 31 August 2021, in final form 15 April 2022)

ABSTRACT: Understanding the contribution of ocean circulation to glacial–interglacial climate change is a major focus of paleoceanography. Specifically, many have tried to determine whether the volumes and depths of Antarctic- and North Atlantic–sourced waters in the deep ocean changed at the Last Glacial Maximum (LGM; ~22–18 kyr BP) when atmospheric pCO_2 concentrations were 100 ppm lower than the preindustrial. Measurements of sedimentary geochemical proxies are the primary way that these deep ocean structural changes have been reconstructed. However, the main proxies used to reconstruct LGM Atlantic water mass geometry provide conflicting results as to whether North Atlantic–sourced waters shoaled during the LGM. Despite this, a number of idealized modeling studies have been advanced to describe the physical processes resulting in shoaled North Atlantic waters. This paper aims to critically assess the approaches used to determine LGM Atlantic circulation geometry and lay out best practices for future work. We first compile existing proxy data and paleoclimate model output to deduce the processes responsible for setting the ocean distributions of geochemical proxies in the LGM Atlantic Ocean. We highlight how small-scale mixing processes in the ocean interior can decouple tracer distributions from the large-scale circulation, complicating the straightforward interpretation of geochemical tracers as proxies for water mass structure. Finally, we outline promising paths toward ascertaining the LGM circulation structure more clearly and deeply.

KEYWORDS: Diapycnal mixing; Meridional overturning circulation; Ocean circulation

1. Introduction

The global ocean's overturning circulation joins the surface to the deep, transports large amounts of heat around the globe, and regulates ocean carbon uptake and release. The overturning circulation contributes approximately 1/2–1/3 of the global equator to pole heat transport (Talley 2003), and the deep ocean contains roughly 60 times more carbon than the atmosphere (Sigman and Boyle 2000). As a result, the overturning circulation plays a primary role in global climate, both today and over the glacial–interglacial cycles of the past (Adkins 2013; Sigman et al. 2010, 2020). While we can observe the modern ocean to understand how circulation impacts global climate, our understanding of past ocean circulation changes relies on geochemical proxy data. It is therefore crucial to understand how tracer distributions record information about the ocean circulation structure, and to determine how the effects of small-scale processes might complicate our interpretations of these tracer distributions.

The modern ocean is proposed to have "figure-eight" circulation structure (Talley 2013). While the figure-eight is admittedly a simplification of the complex pathways subsurface water masses take in the Atlantic (Bower et al. 2019), we find it to be a useful starting point when considering possible circulation changes in the geologic past. North Atlantic Deep Water (NADW) is formed via deep convection in the Nordic, Irminger, and Labrador Seas (Johnson et al. 2019; Bower et al. 2019) and flows southward through the Atlantic basin. When it reaches the Southern Ocean, this water, now mixed with other water masses and called Lower Circumpolar Deep Water (LCDW), upwells as it flows around the Southern Ocean within the Antarctic Circumpolar Current (ACC) (Tamsitt et al. 2017, 2018), moves southward, and eventually reaches the continental shelves of the Weddell and Ross Seas (Fig. 1a). Here LCDW is densified by cooling and brine rejection, and sinks to form Antarctic Bottom Water (AABW), which flows into the Atlantic, Pacific, and Indian Ocean basins. There, the downward diffusion of heat, which is aided by enhanced mixing over rough

All the authors contributed equally to this work.

Supplemental information related to this paper is available at the Journals Online website: https://doi.org/10.1175/JCLI-D-21-0671.s1.

Corresponding author: Frank J. Pavia, fjpavia@caltech.edu

DOI: 10.1175/JCLI-D-21-0671.1

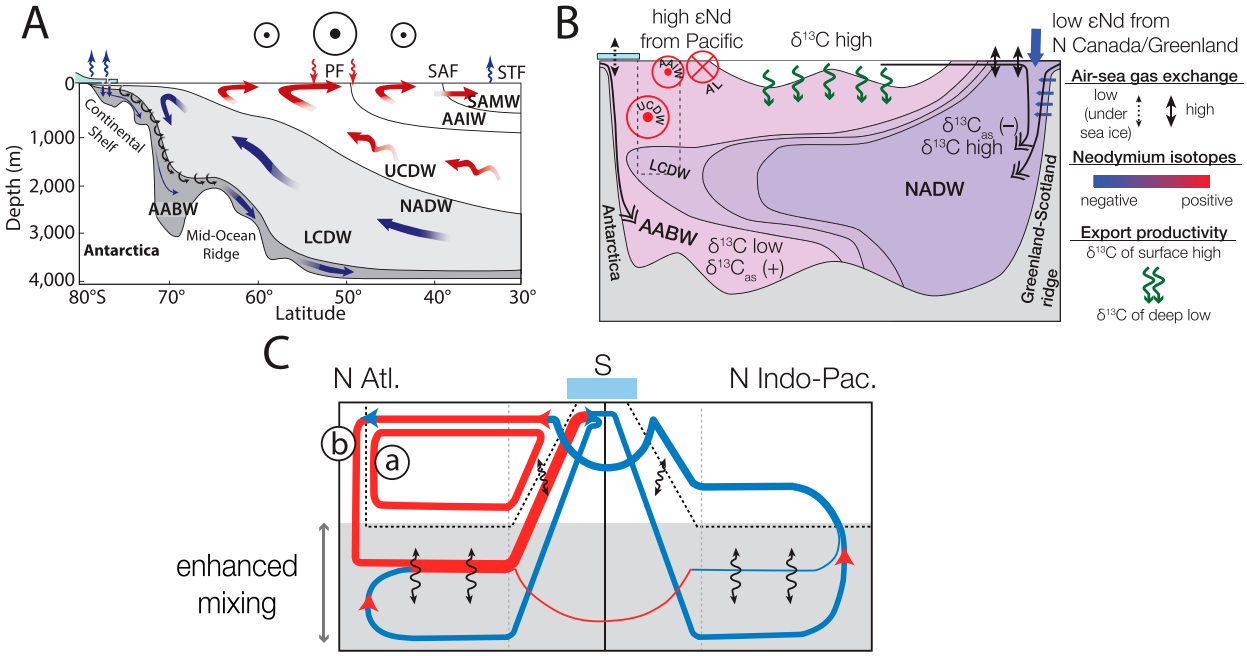

FIG. 1. Modern ocean circulation. (a) Circulation in the Southern Ocean [adapted from Speer et al. (2000)]. Locations of the Subtropical Front (STF), Subantarctic Front (SAF), and Polar Front (PF) are labeled. Blue arrows mark waters that upwell in a region of negative buoyancy forcing (blue arrows at surface), and red arrows mark waters that upwell in a region of positive buoyancy forcing (red arrows at surface). Circles at top denote the Southern Hemisphere westerly winds. Water masses are also labeled (see text for details). (b) Schematic of geochemical and physical processes that affect εNd, δ^{13}C, and $\delta^{13}C_{AS}$ in the Atlantic Ocean. Green wavy arrows represent biological productivity in the surface ocean that fractionates carbon isotopes. Background colors represent εNd values that are affected by weathering of old rocks in northern Canada and Greenland (negative εNd) and young volcanic rocks around the Pacific (positive εNd), which influence Atlantic εNd distributions via mixing through the Southern Ocean [illustrated by red ⊙ and ⊗, which represent Antarctic Intermediate Water (AAIW), Upper Circumpolar Deep Water (UCDW), and Agulhas Leakage (AL)]. (c) Basin-averaged global ocean circulation [adapted from Nadeau et al. (2019) and Nadeau and Jansen (2020)]. Wavy arrows show diapycnal mixing, and gray shaded region represents enhanced vertical mixing in the deep ocean. The loop labeled "a" is predominantly adiabatic: water flows along isopycnals that join the surface of the North Atlantic with the surface of the Southern Ocean. The loop labeled "b" relies on diapycnal mixing in the deep ocean to return deep water to the surface.

topography (Polzin et al. 1997; Waterhouse et al. 2014), causes AABW to upwell across isopycnals. The AABW that flows into the Atlantic upwells back into NADW, but the AABW that flows into the Pacific and Indian oceans can upwell further to form Indian and Pacific Deep Water (IDW/PDW). This water is sufficiently light that when it returns to the Southern Ocean, now called Upper Circumpolar Deep Water (UCDW), it upwells in a region of the Southern Ocean where it becomes less dense due to warming and sea ice melt freshening, thus allowing the meridional overturning circulation to close via northward transport of surface and intermediate waters in the Atlantic (Figs. 1a,c).

In the surface ocean, the process of primary production converts inorganic carbon into organic matter. When this organic matter sinks and is regenerated back to dissolved inorganic carbon via respiration, it is sequestered in the deep ocean, a process known as the biological pump. The global overturning circulation operates on time scales of $O(1000)$ years (Stuiver et al. 1983), providing a mechanism for deeply regenerated CO_2 to be isolated from the atmosphere for long time scales. Therefore through changes in overturning circulation, the deep ocean is thought to exert a strong influence on the pCO_2 of the atmosphere and thus global temperatures. As described above, the North Atlantic and the Southern Ocean are the only two places in the global ocean where deep waters are formed. It is generally thought that changes in both the physical overturning circulation and the biological pump are necessary to achieve full glacial–interglacial atmospheric pCO_2 changes (Sarmiento and Toggweiler 1984; Siegenthaler and Wenk 1984; Knox and McElroy 1984; Toggweiler 1999; Watson and Naveira Garabato 2006; Sigman et al. 2010; Skinner et al. 2010), although a recent study challenges whether circulation changes are needed (Khatiwala et al. 2019).

In addition to changes in the overturning circulation rate (see, e.g., Kwon et al. 2012), changes in ocean overturning circulation geometry may also contribute to deep ocean carbon sequestration. Our understanding of water mass structure during the Last Glacial Maximum (LGM) is largely based on meridional sections of chemical tracers with distinct values in northern- and southern-sourced deep water endmembers (Fig. 1b). Based on these reconstructions, some have suggested that the LGM (~22–18 kyr BP) ocean had a two-cell circulation structure, with greater separation between the upper and lower cells compared with the modern ocean circulation (Curry and Oppo

2005; Lund et al. 2011; Ferrari et al. 2014). This structure could have allowed for longer deep ocean residence times and more carbon sequestration in the glacial ocean (Burke et al. 2015; Skinner et al. 2017), and it could have contributed a substantial portion of the documented atmospheric pCO_2 draw-down at the LGM. However, recent analyses using different paleocean circulation tracers suggest much more modest changes in water mass distributions (Howe et al. 2016; Pöppelmeier et al. 2020), challenging the means by which the glacial deep ocean contributed to atmospheric pCO_2 draw-down. To fully understand the role of the ocean in glacial–interglacial climate change, it is important to understand these apparent discrepancies in the interpretation of paleoproxy measurements and to determine the overturning circulation structure at the LGM.

Ocean mixing plays a first-order role in determining ocean circulation structure, and it also directly impacts ocean tracer distributions. Recent work suggests that the strength of diapycnal mixing, which moves tracers across constant density surfaces, and the strength of isopycnal mixing, which moves tracers along constant density surfaces, may have been different at the LGM (Wilmes et al. 2019; Jones and Abernathey 2019). Ocean stratification also likely changed at the LGM, influencing the strength of vertical transport by diapycnal mixing. Temporal changes in mixing strength and spatial heterogeneity in ocean mixing significantly complicate the relationship between ocean circulation geometry and ocean tracer distributions, as explored in sections 2b and 4b.

Given the central role that deep ocean circulation changes play in many explanations for glacial–interglacial climate change, it is not surprising that this subject has interested physical oceanographers as well as paleoceanographers. Several modeling studies have sought to provide a physical basis for paleo observations that suggest the presence of a shoaled upper cell at the LGM (Curry and Oppo 2005; Galbraith and de Lavergne 2018), possibly driven by changes in Southern Ocean sea ice (Ferrari et al. 2014; Watson et al. 2015; Jansen and Nadeau 2016; Marzocchi and Jansen 2017; Sun et al. 2018; Nadeau et al. 2019; Baker et al. 2020; Sun et al. 2020), terrestrial ice inputs (Miller et al. 2012), and/or increased density stratification between the upper and lower cells (Lund et al. 2011; Jansen 2017). While these studies provide crucial assessments of the physical realism of proposed glacial circulation structures, they are often difficult to compare with observations because they focus on differences in the large-scale circulation between the modern ocean and the LGM. We believe that faster progress will be made if physical oceanographers work together with paleoceanographers to assess what circulation geometries are possible given constraints from paleoproxy data: here we take new steps on that journey. We hope this paper can provide a stronger physical intuition for paleoceanographers to apply as they use geochemical techniques to ascertain the ocean circulation structure in the past, and increase understanding of paleoceanographic concepts within the physical oceanographic community.

In this paper, we suggest that deep ocean mixing processes may exert critical controls on reconstructed tracer distributions during the LGM, and outline alternative methods of utilizing tracer data to understand LGM circulation changes. In section 2 we discuss the physical mechanisms by which the overturning circulation could have shoaled and mixing could have changed at the LGM, and in section 3 we review the systematics of paleo proxies that are commonly used for reconstructing ocean circulation geometry. In section 4 we discuss different LGM circulation scenarios that are physically based and can explain the available proxy data. In section 5 we offer suggestions of fruitful new avenues of exploration, which we hope will clarify the geometry of the ocean circulation at the LGM.

2. Ocean circulation

a. *Possible shoaling of the MOC's upper cell*

Meridional transport in the Southern Ocean is created by the slight imbalance between two competing processes: wind-driven Ekman flow in the frictional surface and bottom boundary layers, which acts to steepen isopycnal surfaces, and baroclinic eddies, which form in response to steepened isopycnal surfaces and act to reduce isopycnal slopes (Marshall and Radko 2003; Marshall and Speer 2012). The resulting advective meridional transport by the residual flow is primarily oriented along isopycnals. Buoyancy fluxes at the surface of the Southern Ocean cause transport across isopycnals in the surface mixed layer. Water that upwells in a region of positive buoyancy flux moves northward at the surface, and water that upwells in a region of negative buoyancy flux moves southward at the surface, as shown in Fig. 1a. Thus the pattern of Southern Ocean buoyancy fluxes impacts whether water moves northward or southward in the Southern Ocean, influencing the pathway of the MOC.

The surface buoyancy flux comprises heat and freshwater components, which are exchanged between the ocean and atmosphere and/or between the ocean and overlying sea ice or terrestrial ice. Abernathey et al. (2016) and Pellichero et al. (2018) have demonstrated that water mass transformations south of the polar front are dominated by sea ice–driven surface buoyancy fluxes. Water mass transformation into denser classes occurs in coastal polynyas around Antarctica, where sea ice formation leads to buoyancy loss via brine rejection. As sea ice is redistributed by winds and currents, it eventually melts at a more northern latitude than it formed, leading to buoyancy gain and water mass transformation into lighter buoyancy classes (Saenko et al. 2003; also see red arrows in Fig. 1a herein).

Sea surface temperatures in the LGM Southern Ocean were lower (Ho et al. 2012) and sea ice extended farther north (Gersonde et al. 2005). Hence, the latitudinal position of the boundary between positive and negative buoyancy fluxes probably moved northward at the LGM. Ferrari et al. (2014) presented a theory that suggests that moving this boundary farther north will shoal the isopycnals associated with this boundary. They argue that Southern Ocean isopycnal slopes s are approximately equal to

$$s \simeq \frac{\tau_0}{\rho_0 f K}, \tag{1}$$

where τ_0 is the time-mean zonal wind stress, ρ_0 is the surface reference density, K is the eddy transfer coefficient, and f is the Coriolis parameter. Isopycnal surfaces are generally flat in the ocean basins to the north of the Southern Ocean. Hence,

if the growth of Antarctic sea ice pushes surface density contours northward, the isopycnals in the ocean interior associated with these contours will shoal if isopycnal slopes remain constant through time (see Ferrari et al. 2014 and Fig. 4 therein).

Ferrari et al. (2014) argued that this happened during the LGM, and that isopycnals associated with buoyancy gain were shoaled above 2000-m depth. Vertical ocean mixing is weaker above 2000 m and stronger below 2000 m due to the presence of rough topography at depth (Ledwell et al. 2000). Ferrari et al. (2014) suggest that diapycnal transport across the isopycnal that separates positive and negative buoyancy flux regions at the surface of the Southern Ocean would have been reduced, causing the upper cell of the MOC to separate from the lower cell of the MOC. Because of its clarity, the Ferrari et al. (2014) paper has been widely read and cited in the paleo-oceanographic community.

Recent work by Sun et al. (2018), Nadeau and Jansen (2020), and Baker et al. (2021) has shown that the Ferrari et al. (2014) hypothesis is an incomplete view of the ocean dynamics at the LGM, because it focuses on the sign of surface buoyancy forcing as the primary control on ocean stratification, and does not consider the effects of subsurface Southern Ocean mixing, the effects of changes in global diapycnal mixing, or how changes in the magnitude of Southern Ocean buoyancy loss might further impact the stratification. The AMOC comprises two components: an adiabatic component, which upwells in the Southern Ocean and is directly driven by the strong zonal winds there (loop a in Fig. 1c), and a diabatic component, in which water upwells across isopycnals, primarily driven by small-scale vertical mixing in the Indian and Pacific Oceans (loop b in Fig. 1c; Jones and Cessi 2016; Ferrari et al. 2017). Sun et al. (2018) shows that diabatic upwelling in the Southern Ocean is also important. The depth of the adiabatic component of the AMOC is directly linked to the outcrop latitude of the isopycnal that separates positive and negative buoyancy flux regions at the surface of the Southern Ocean. The diabatic component of the AMOC usually extends deeper into the water column than the adiabatic component, and its strength and depth are set by multiple factors, including the strength of cross-isopycnal upwelling due to small-scale mixing and the density of AABW formed in the Southern Ocean (Nadeau and Jansen 2020).

Nadeau and Jansen (2020) and Baker et al. (2021) show that increasing the strength of diapycnal mixing deepens the upper cell of the overturning circulation. An increase in the strength of diapycnal mixing at the LGM seems likely and is discussed further in section 2b. Jansen and Nadeau (2016), Nadeau et al. (2019), Nadeau and Jansen (2020), and Baker et al. (2021) found that increasing the buoyancy loss around Antarctica (due to an increase in sea ice formation at the LGM) increases the stratification, which inhibits this cross-isopynal transport. This reduces the AMOC transport due to the diabatic component of the circulation, leading to shoaling of the AMOC. Taken together, this recent work demonstrates that multiple factors are involved in setting the depth of the AMOC, and calls into question the earlier consensus view that sea ice extent is the main control on AMOC depth.

b. *Possible changes to ocean mixing*

While much attention has been paid to large differences in circulation geometry between the modern and LGM oceans, significant differences in small-scale ocean processes like mixing are also probable in some key locations. Most notably, a 120- to 130-m drop in sea level at the LGM may have caused an increase in tidal dissipation in the deep ocean, particularly in the North Atlantic (Arbic et al. 2004; Egbert et al. 2004; Griffiths and Peltier 2009; Green 2010; Schmittner et al. 2015; Wilmes et al. 2019). Vertical diffusivity is controlled by both tidal energy dissipation and by stratification as follows:

$$\kappa_z = \Gamma \frac{\epsilon}{N^2}, \text{ where } N = \sqrt{\frac{-g}{\rho_0}\frac{\partial \rho}{\partial z}}, \tag{2}$$

where κ_z is the vertical diffusivity, Γ is the mixing efficiency, ϵ is the rate of tidal energy dissipation, and N^2 is the buoyancy frequency, which is a measure of ocean stratification. In idealized models, higher vertical diffusivities lead to deepening of the upper cell of the AMOC, particularly in the North Atlantic (Baker et al. 2021). For a constant abyssal ocean stratification, increased tidal dissipation at the LGM would lead to larger vertical diffusivities in the abyssal ocean. Increased ocean stratification in the deep ocean may have partially compensated for the increase in tidal energy dissipation, leading to a more modest increase in the vertical diffusivity of the deep ocean. On the other hand, increased tidal mixing may itself decrease the ocean stratification. Wilmes et al. (2019) tested a range of ocean stratifications from Muglia et al. (2018), including some scenarios with saltier AABW. They found the buoyancy frequency was relatively insensitive to AABW salinity, concluding that the vertical diffusivity of the abyssal Atlantic was probably larger at the LGM.

Larger vertical mixing probably causes more exchange between the upper and abyssal cells of the overturning circulation: this is explored further in section 4b. Many Paleoclimate Modeling Intercomparison Project phase 3 and 4 (PMIP3 and PMIP4) models parameterize tidal mixing using a sensible parameterization like St. Laurent et al. (2002). These models often use high-resolution tidal models to generate a mixing distribution, which is then applied to the ocean in the fully coupled production run of the climate model.

Recent work by Ferrari et al. (2016) and Callies and Ferrari (2018) highlights that when vertical mixing increases toward the bottom of the ocean, this can cause downward velocities in the interior, with upward velocities along the sloping boundaries of the ocean. This sort of vertical mixing profile may lead to larger diapycnal tracer transport into the deep ocean (Jones and Abernathey 2021). This new paradigm highlights the role of lateral fluxes in bringing water close to rough topography, where diapycnal mixing is strongest (Mashayek et al. 2017). The complex relationship between the large-scale flow and patterns of small-scale mixing may complicate the interpretation of paleotracer estimates because these are only available for water masses that are close to topography.

An additional (though smaller) change in ocean mixing might have been caused by changes to the surface wind stress over the Southern Ocean. Evidence for such a change is mixed

(Stuut et al. 2002; Kim et al. 2003; Kohfeld et al. 2013; Gottschalk et al. 2019). Stronger surface winds drive higher eddy kinetic energy in the upper ocean, which is associated with larger isopycnal mixing (Abernathey and Ferreira 2015). Higher isopycnal mixing rates in the Southern Ocean are associated with more southern-sourced water reaching the deep ocean, particularly in the deep Pacific (Jones and Abernathey 2019). Isopycnal mixing may be important for explaining deep ocean tracer distributions at the LGM (Burke et al. 2015). This effect is unlikely to be well represented in PMIP3 and PMIP4 models: detailed study of isopycnal mixing is in its early stages, so many paleoclimate model simulations still specify an isopycnal mixing field that is constant in time (see, e.g., Rackow et al. 2019; Lin et al. 2020; Chassignet et al. 2020), despite findings from physical oceanographers that isopycnal mixing rates are likely not constant (e.g., Gent 2016).

3. Background on proxy systematics

In lieu of direct observations of mixing rates and overturning streamfunctions, chemical oceanographers and paleoceanographers turn toward observations of tracers. Chemical species in the ocean are sensitive to the physical transport phenomena described in the preceding sections, as well as biogeochemical transformations that can add and remove these tracers from a given water parcel as it flows in the ocean.

A simple physical and biogeochemical equation (the conservation equation) describes the time rate of change of a chemical species at a given location:

$$\frac{\partial C}{\partial t} = -\mathbf{U} \cdot \nabla C + \nabla \cdot (\mathbf{D} \cdot \nabla C) + J(C). \tag{3}$$

The first term in this equation describes the change in concentration due to advective flux divergence ($\mathbf{U}$) acting on the tracer concentration C, the second term represents the flux divergence due to diffusive processes ($\mathbf{D}$), while the third term $J(C)$ represents nonconservative biogeochemical sources and sinks. In this paper, where we are primarily interested in the meridional and vertical changes in tracer concentrations, we consider the two-dimensional form of this equation between two isopycnal surfaces ζ_1 and ζ_2 where $\zeta_2 - \zeta_1 = h$ is the distance in meters between the two isopycnals:

$$\underbrace{\frac{\partial(hC)}{\partial \tilde{t}}}_{\text{tendency}} = \underbrace{-\frac{\partial(VC)}{\partial \tilde{y}}}_{\text{(along-)isopycnal advection}} \underbrace{-\,[\Omega C]_{\zeta_1}^{\zeta_2}}_{\text{diapycnal advection}} + \underbrace{\frac{\partial}{\partial \tilde{y}}\left(K_h h \frac{\partial C}{\partial \tilde{y}}\right)}_{\text{along-isopycnal diffusive transport}} + \underbrace{\left[K_z \frac{\partial C}{\partial z}\right]_{\zeta_1}^{\zeta_2}}_{\text{diapycnal diffusive transport}} + \underbrace{\int_{\zeta_1}^{\zeta_2} J(C)\, dz}_{\text{source or sink}}, \tag{4}$$

where $(\tilde{x}, \tilde{y}, \tilde{b}, \tilde{t})$ are buoyancy coordinates, as described in Young (2012). This equation describes the effects of isopycnal advection by the meridional velocity, integrated between ζ_1 and ζ_2 (V; $\mathrm{m^2\,s^{-1}}$); diapycnal advection by the diapycnal velocity Ω; $\mathrm{m\,s^{-1}}$); isopycnal diffusion by the isopycnal diffusivity (K_h; $\mathrm{m^2\,s^{-1}}$); vertical diffusion by the vertical diffusivity (K_z; $\mathrm{m^2\,s^{-1}}$); and sources and sinks due to nonconservative fluxes $\{J(C); [C]\ \mathrm{s^{-1}}\}$ on a tracer C. These are averaged in the zonal direction over the whole ocean basin. The meridional volume transport (V), the isopycnal diffusivity (K_h), and the tracer concentrations (C) are assumed to be vertically uniform between the two isopycnals. A simple explanation of this coordinate system, as well as a proof of the equation above, is given in the online supplemental material. Even at steady state (i.e., when the tendency term is zero), five different processes act to set the tracer concentration at any point, so isopycnal advection may not always be the most important factor for determining deep ocean tracer concentrations. This two-dimensional simplification also neglects zonal advective and diffusive fluxes, which may be important in the real ocean.

Tracers that have either no subsurface biogeochemical sources or sinks (e.g., salinity) or are corrected for their biogeochemical transformations via stoichiometric relations to other tracers (e.g., PO_4^*; Broecker et al. 1998) are considered to be conservative [i.e., the fifth term in Eq. (5) equals zero]. When two water masses with different initial concentrations of a conservative tracer undergo binary mixing, the tracer concentration of the mixture reflects the proportional contribution from each water mass. Thus, provided that the initial (or "endmember") tracer concentration for water masses is known, measurements of that tracer can be used to quantify the relative proportions of the two source water masses, for example NADW and AABW. This approach of course relies on the assumption that the deep Atlantic is mostly made up of these two water masses, and that there are not additional water masses in the tracer budget of the deep Atlantic.

A wide variety of proxies have been used to study the overturning circulation in the geologic past, but conservative tracers are relatively rare in paleoceanography. Here we focus on three tracers, with varying degrees and modes of conservativeness, that have been used to reconstruct water mass geometry of the deep Atlantic Ocean since the LGM: stable carbon isotopes of dissolved inorganic carbon ($\delta^{13}C_{DIC}$), the air–sea exchange component of carbon isotopes ($\delta^{13}C_{AS}$), and the seawater neodymium isotopic composition (εNd) (schematically introduced in Fig. 1b). We recognize that other tracers such as radiocarbon (^{14}C) (e.g., Stuiver et al. 1983; Key et al. 2004) and $^{231}Pa/^{230}Th$ (e.g., McManus et al. 2004; Gherardi et al. 2009; Lippold et al. 2012) have also been extensively used to examine ocean circulation in the past, but as these tracers are typically interpreted to contain more information about circulation strength rather than geometry, we have omitted them from this paper. An interesting

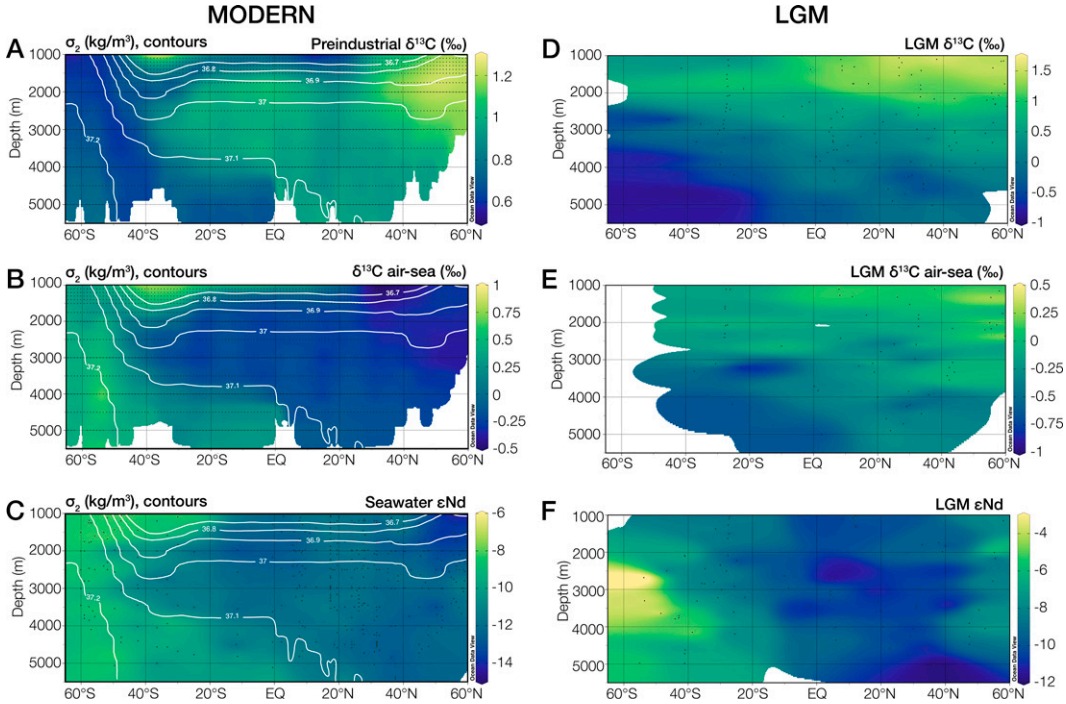

FIG. 2. Atlantic Ocean section plots for the Modern and Last Glacial Maximum. (a),(b) The preindustrial $\delta^{13}C_{DIC}$ climatology of Eide et al. (2017) is used, and data from the Atlantic Ocean zonally averaged between 45° and 10°W are shown. Calculation of $\delta^{13}C_{AS}$ in (b) was performed by merging the $\delta^{13}C_{DIC}$ climatology with the World Ocean Atlas 2018 phosphate grid, and calculating $\delta^{13}C_{AS}$ using Eq. (6). (c) The seawater εNd database compiled by Du et al. (2020) is used. Contours in (a)–(c) show the potential density anomaly in kg m^{-3} referenced to a pressure of 2000 db (ρ_2). (d)–(f) Analogous sections reconstructed for the LGM. Data in (d) and (e) come from the compilations of Oppo et al. (2018), while data in (f) come from the LGM compilation of authigenic εNd from Du et al. (2020). The plots in (d)–(f) include all Atlantic basin data from these compilations, regardless of zonal location. Note that the color bars differ between left and right panels, because endmember values for these proxies differ between the modern and LGM oceans.

recent study suggests that radiocarbon distributions may be more sensitive to AMOC depth than previously thought (Muglia and Schmittner 2021). This is a significant departure from the traditional interpretation and warrants further investigation.

a. *Stable carbon isotopes*

Because ^{13}C is marginally heavier than ^{12}C, chemical and physical processes act on the two isotopes at slightly different rates. The ratio of ^{13}C to ^{12}C of dissolved inorganic carbon (DIC) in seawater, which is expressed in delta notation ($\delta^{13}C_{DIC}$) as the parts per thousand variation with respect to a standard, is altered by photosynthesis, respiration of organic matter, and air–sea gas exchange. Below we describe how each of these processes affect this ratio.

1) $\delta^{13}C$ AND ORGANIC MATTER

Phytoplankton preferentially take up ^{12}C. Thus, as phytoplankton photosynthesize and grow, they cause nutrients to become more completely utilized at the sea surface, and cause the remaining $\delta^{13}C_{DIC}$ of surface seawater to become heavier. Surface waters subducting into the interior with more complete nutrient utilization will have heavier $\delta^{13}C_{DIC}$ at the time of subduction, while waters subducting with high initial nutrient concentrations will have lighter $\delta^{13}C_{DIC}$. As subsurface waters age, they gain DIC via the remineralization of particulate and dissolved organic carbon, both of which are isotopically light. Thus, the $\delta^{13}C_{DIC}$ of a water parcel decreases with ventilation age, as remineralization occurs during aging.

In the modern Atlantic, there is a roughly 1‰ difference between AABW and NADW. AABW has an initial $\delta^{13}C_{DIC}$ value of ~0.4‰ and NADW has $\delta^{13}C_{DIC}$ of 1.3‰ (Fig. 2a). Because of the relatively fast circulation time scales of the deep Atlantic and low carbon remineralization fluxes in deep waters, a binary mixing formulation can be used to determine the fraction of NADW (f_{NADW}) present using $\delta^{13}C_{DIC}$ measurements:

$$f_{NADW} = \frac{\delta^{13}C_{DIC}^{meas} - \delta^{13}C_{DIC}^{south}}{\delta^{13}C_{DIC}^{north} - \delta^{13}C_{DIC}^{south}}, \quad (5)$$

where the superscript "meas" indicates the measured $\delta^{13}C_{DIC}$ of a particular water sample, and the superscripts "north" and "south" refer to the endmember $\delta^{13}C_{DIC}$ values. This equation is a slight simplification, as it neglects DIC concentration differences between water masses. However, since DIC concentration differences are much smaller than $\delta^{13}C_{DIC}$ differences, this simplification is reasonable when considering mixing of NADW and AABW.

2) δ^{13}C AND AIR–SEA EXCHANGE

Carbon isotopes in seawater are also affected by air–sea gas exchange. There are three air–sea exchange processes of importance: 1) temperature-dependent equilibrium fractionation (heavier $\delta^{13}C_{DIC}$ at colder temperatures), 2) fractionation due to the degree of air–sea equilibration (heavier $\delta^{13}C_{DIC}$ for more complete equilibration), and 3) net gain/loss of DIC due to gas exchange (heavier $\delta^{13}C_{DIC}$ for net DIC loss) (Lynch-Stieglitz et al. 1995). These combined effects alter the $\delta^{13}C_{DIC}$ composition during air–sea interaction.

Phosphate (PO_4) is a key nutrient required for biological activity, and it can thus be used to isolate the biological effects on $\delta^{13}C_{DIC}$ from the physical effects. The slope of the modern ocean biological $\delta^{13}C_{DIC}$–PO_4 relationship has a value of −1.1, which is dictated by the photosynthetic fractionation of carbon isotopes, the ratio of carbon to phosphorus in organic matter, and the mean ocean concentration of DIC (see the supplemental text in the online supplemental material). The intercept is chosen such that the physical air–sea component of δ^{13}C ($\delta^{13}C_{AS}$) in the deep Indo-Pacific has a value of 0.

$$\delta^{13}C_{AS,modern} = \delta^{13}C_{DIC} + 1.1[PO_4] - 2.75. \quad (6)$$

This equation corrects the measured δ^{13}C value for biological effects, therefore leaving an isotope signature that represents only physical processes (temperature, air–sea equilibration, and net DIC exchange).

The deep Atlantic Ocean is characterized by two distinct $\delta^{13}C_{AS}$ endmembers (Fig. 2b; see also supplemental Fig. 1A in the online supplemental material). NADW has $\delta^{13}C_{AS} = -0.5‰$ and AABW has $\delta^{13}C_{AS} = 0.4‰$–$0.5‰$ (Eide et al. 2017; Lynch-Stieglitz et al. 1995; Mackensen 2012). These endmember $\delta^{13}C_{AS}$ values are driven by differences in air–sea equilibration temperature (warmer for NADW, colder for AABW) and CO_2 uptake (invasion of atmospheric CO_2 in the North Atlantic, and evasion of CO_2 from the Southern Ocean). To reconstruct $\delta^{13}C_{AS}$, paleoceanographers must use proxy measurements for past ocean PO_4. The micronutrient Cd bears striking similarity to PO_4 (Elderfield and Rickaby 2000; Boyle 1988; Middag et al. 2018), and the modern relationship between these two species can be used to reconstruct PO_4 in the past, where past ocean Cd is calculated using measurements of the Cd/Ca ratio in foraminifera (see the supplemental text for additional detail). Calculations of past ocean $\delta^{13}C_{AS}$ also must take into account changes in the mean ocean [DIC] and δ^{13}C, and photosynthetic fractionation.

Assuming known changes in mean ocean terms, $\delta^{13}C_{AS}$ values should be a conservative tracer in the ocean interior (Charles et al. 1993; Lynch-Stieglitz and Fairbanks 1994). Similarly to $\delta^{13}C_{DIC}$, the distinct values of $\delta^{13}C_{AS}$ between NADW and AABW allow for a binary mixing formulation to determine the fraction of NADW present in a water parcel:

$$f_{NADW} = \frac{\delta^{13}C_{AS}^{meas} - \delta^{13}C_{AS}^{south}}{\delta^{13}C_{AS}^{north} - \delta^{13}C_{AS}^{south}}, \quad (7)$$

where the superscript "meas" indicates the calculated $\delta^{13}C_{AS}$ value from the measured $\delta^{13}C_{DIC}$ and [PO_4] of a particular water sample [using Eq. (6) or its glacial equivalent], and the superscripts "north" and "south" refer to the endmember $\delta^{13}C_{AS}$ values.

b. Authigenic neodymium isotopes (εNd)

Another commonly applied tracer for reconstructing water mass changes in the geologic past is the neodymium isotope ratio εNd, the ratio of ^{143}Nd to ^{144}Nd as the parts per ten thousand variation with respect to the composition of the chondritic reservoir (Jacobsen and Wasserburg 1980). Seawater acquires neodymium from the input of lithogenic material, either at the surface, through dust deposition and fluvial input (Goldstein and Hemming 2003; Siddall et al. 2008), or at the seafloor by benthic fluxes of Nd out of sedimentary porewaters (e.g., Haley et al. 2017; Jeandel 2016). Away from regions of external Nd input or exchange, the seawater isotopic composition is largely conserved. Thus, the εNd value of seawater reflects the εNd of the local source rocks that deliver this Nd to the ocean and mixing between water masses with different εNd compositions. Neodymium isotope ratios are set by decay of ^{147}Sm to ^{143}Nd with a half-life of 106 Ga, and therefore reflect the initial Sm/Nd ratio of a rock and the amount of time it has spent in the continental crust. Because εNd varies significantly between old, continental rocks found around the North Atlantic and young, volcanic rocks found around the North Pacific, individual basins and water masses have unique εNd signatures reflecting their inputs, and relative proportions of waters from Pacific and Atlantic εNd endmembers (e.g., Goldstein and Hemming 2003, and references therein).

In the modern Atlantic Ocean, NADW has an εNd of about −13.5 (Lambelet et al. 2016), while AABW has an εNd of −8 (van de Flierdt et al. 2016; Fig. 2c). Unlike carbon isotopes and cadmium, which are directly taken up into benthic foraminiferal calcite, deepwater εNd is primarily recorded in authigenic sedimentary phases, such as ferromanganese coatings. This necessitates that authigenic signals are fully separated from detrital signals (i.e., local continental input) when sedimentary records are analyzed to reconstruct past ocean εNd. In the past, the North Atlantic εNd endmember composition may have been affected by changes in the supply of continental material to the ocean (Zhao et al. 2019), the strength or pathway of boundary currents, and/or changes in the zonal location of deep-water formation. Deep water that passes through the Labrador Sea tends to have more negative εNd values than NADW that is formed in the Greenland, Iceland, and Norwegian Seas. Hence, a reduction in deep-water formation in the Labrador Sea, or a reduction in NADW transit through the Labrador Sea, could lead to an increase in the northern endmember εNd value. In the interior Atlantic, the εNd values of NADW and AABW are modified partially by benthic Nd fluxes but, due to the advection-dominated circulation regime, these water masses primarily mix conservatively (Haley et al. 2017; Du et al. 2020). Assuming conservative mixing, the fraction of NADW can be calculated from Nd isotope measurements using the following binary mixing equation (e.g., Howe et al. 2016):

$$f_{\mathrm{NADW}} = \frac{R_S[\mathrm{Nd}]_S - R_{\mathrm{Meas}}[\mathrm{Nd}]_S}{R_{\mathrm{Meas}}([\mathrm{Nd}]_N - [\mathrm{Nd}]_S) - R_N[\mathrm{Nd}]_N + R_S[\mathrm{Nd}]_S}, \tag{8}$$

where R denotes the εNd value of an endmember or measurement and [Nd] is the Nd concentration of an endmember, where subscripts S and N indicate southern-source and northern-source, respectively, and "Meas" is the measured value for a given sample consisting of a mixture of NADW and AABW. There is no proxy for past ocean [Nd], so this is generally assumed to be constant at the modern ocean values.

c. *Proxy preservation and fidelity*

In addition to the systematics of proxy behavior in seawater, it is also necessary to account for alteration of proxy signals in microenvironments as they are recorded and/or after they are incorporated into sediments and buried. Such processes are well known to bias records and cause them to deviate from bulk seawater. For δ^{13}C, there are two common ways that this occurs: either via the Mackensen effect (Mackensen et al. 1993) wherein organic matter respiration at the sediment–water interface decreases the δ^{13}C values recorded by benthic foraminifera within that microenvironment relative to the surrounding seawater, or by vertical migration of benthic foraminifera within the sediment column (Gottschalk et al. 2016), which also tends to bias recorded values toward lower values relative to surrounding seawater (Schmittner et al. 2017). For $\delta^{13}C_{AS}$, the same biases exist as for δ^{13}C, but there may be additional complications arising from using Cd/Ca ratios to reconstruct PO_4, which is sensitive to seawater saturation state with respect to calcite and dissolution (Marchitto and Broecker 2006, and references therein). Finally, authigenic εNd records can also be biased in either direction by overprinting within pore water microenvironments (Blaser et al. 2019). This occurs when detrital material dissolves and then reprecipitates in an authigenic phase.

In an attempt to overcome these issues and their possible spatial heterogeneity, in this paper we compile all available data for the LGM Atlantic for each of these three proxies, without attempting to filter the data for preservation issues.

4. Discussion

If nonconservative fluxes are small or can be ignored, then physical transport by advection and eddy diffusion governs the distribution of a tracer in the ocean interior. Tracers with this characteristic thus have their concentrations or isotope ratios controlled by admixture of water masses with different initial compositions, or endmembers. The εNd and $\delta^{13}C_{AS}$ proxies are considered to be largely conservative in the deep Atlantic (Du et al. 2020; Haley et al. 2017; Lynch-Stieglitz et al. 1995; Oppo et al. 2018). Since these tracers have distinct values in subducting NADW and AABW (see next section), measuring their values downcore allows for the reconstruction of the fraction of those two water masses present at a given location, assuming binary mixing between NADW and AABW.

Application of these principles qualitatively (Duplessy et al. 1988; Curry and Oppo 2005) and quantitatively (Piotrowski et al. 2004; Howe et al. 2016; Pena and Goldstein 2014; Pöppelmeier et al. 2020) is one of the primary ways that changes in water mass structure in the paleo Atlantic Ocean has been reconstructed. The two most critical assumptions underlying the application of these proxies are 1) limited effects of nonconservative behavior of the tracer and 2) accurate knowledge of the NADW and AABW endmembers in the binary mixing equations.

We identify an additional complication in interpreting sections of paleoceanographic data in terms of changing water mass structure: the effects of ocean mixing. Specifically, changes in vertical mixing rates [the diapycnal diffusive transport term in Eq. (5)] may cause large changes in the spatial distributions of tracers and only modest changes in overturning circulation outside the North Atlantic. Below, we detail the conventional use of tracer sections to delineate Atlantic circulation geometry, show how conservative tracers purely depend on circulation streamfunctions in PMIP models, and outline paths forward to reconstruct paleo Atlantic water mass geometry that take into account changes in ocean vertical mixing.

a. *Observational evidence*

Perhaps the most well-established evidence in support of shoaled NADW at the LGM has come from comparing meridional sections of modern seawater $\delta^{13}C_{DIC}$ and LGM benthic foraminiferal δ^{13}C (Duplessy et al. 1988; Curry and Oppo 2005; Oppo et al. 2018). These data show striking differences in δ^{13}C distributions in the LGM compared to modern seawater (Fig. 2d). Reconstructed LGM data from the western Atlantic show deep waters with more depleted δ^{13}C values that penetrate into the northern part of the basin and a 500–1000-m shoaling of δ^{13}C-enriched water, generally interpreted to be the glacial version of NADW [often called Glacial North Atlantic Intermediate Water (GNAIW)] (Fig. 2d).

More recently, some studies have challenged the interpretation that δ^{13}C changes at the LGM are indicative of major water mass reorganizations, due to the nonconservative behavior of δ^{13}C. Gebbie (2014) used a steady-state model of the ocean circulation that takes into account both modern seawater observations and paleoproxy data. His steady-state solution showed that while the core of NADW shoaled during the LGM, the depth at which NADW and AABW were a 50–50 mixture remained unchanged. The apparent shoaling of the NADW could be explained by an increase in the respired nutrient content of glacial NADW rather than a change in circulation. Using the same modeling framework with additional data, Oppo et al. (2018) concluded that the core of NADW shoaled by ~500 m at the LGM, with a strong reduction in the NADW fraction in the deepest North Atlantic. This is roughly half of what was suggested in earlier studies (e.g., Curry and Oppo 2005; Lund et al. 2011).

Given the potential for changes in nutrient contents to confound the use of δ^{13}C as a conservative tracer, other studies have turned to $\delta^{13}C_{AS}$, which corrects for the nonconservative remineralization effects on δ^{13}C using Cd as a proxy for phosphate.

Marchitto and Broecker (2006) compiled benthic foraminiferal $\delta^{13}C$ and Cd/Ca measurements from the LGM Atlantic, finding very low $\delta^{13}C_{AS}$ values associated with glacial AABW penetrating into the deep North Atlantic. The authors also argued for a shoaling of LGM NADW, based on observations of high $\delta^{13}C_{AS}$ from 1000 to 2000 m throughout the Atlantic, but acknowledged that incomplete understanding of endmember $\delta^{13}C_{AS}$ values for NADW, AABW, and AAIW hindered unique interpretation of this signal.

Indeed, Gebbie (2014) and Oppo et al. (2018) included $\delta^{13}C_{AS}$ in their data-constrained steady-state modeling efforts. They noted that since $\delta^{13}C_{AS}$ has fairly large errors (0.3‰), and the AAIW and NADW endmembers seem to converge during the LGM toward 0, discriminating between AAIW and NADW in the upper LGM Atlantic is difficult. Only the inclusion of new depth transect $\delta^{13}C_{AS}$ data by Oppo et al. (2018) allowed for the delineation of vertical gradients in $\delta^{13}C_{AS}$ in the LGM western Atlantic (Fig. 2e). The steady-state solution of Oppo et al. (2018), which finds 500 m of NADW shoaling, requires a unique $\delta^{13}C_{AS}$ signature in Nordic seas–derived NADW formed by open ocean convection, but $\delta^{13}C_{AS}$ has not yet been measured from this source region. Additionally, few data are yet available on LGM $\delta^{13}C_{AS}$ from sediment cores south of 40°S (potentially related to preservation issues; see section 3c). A general paucity of data and difficulty inferring glacial endmembers are the main factors inhibiting broad conclusions about LGM Atlantic water mass structure from $\delta^{13}C_{AS}$.

The third tracer often used to assess whether NADW shoaled at the LGM is εNd. Unlike $\delta^{13}C$ and $\delta^{13}C_{AS}$, most studies measuring εNd have argued for no major changes in LGM Atlantic water mass geometry, and compiled LGM εNd shows a similar meridional depth structure as today, with very negative ($\varepsilon Nd < -10$) filling the deep North Atlantic (Fig. 2f). Howe et al. (2016) attempted to quantify the change in NADW present in the deep Atlantic, using an approach similar to Eq. (9). They conduct a sensitivity analysis using one site at 4500 m in the North Atlantic (Roberts et al. 2010) and find between 50% and 100% NADW at that depth, depending on the isotopic composition of the northern endmember and the relative neodymium concentrations of the northern and southern endmembers (a component of the endmember calculation for which there is no paleo proxy). The results of Howe et al. (2016) were further supported by a study in the southwest Atlantic by Pöppelmeier et al. (2020). These authors highlighted the conflicting water mass geometries that arise from using $\delta^{13}C$ versus εNd as a water mass proxy. Du et al. (2020) used a box model of the global ocean to examine changes in the mixing ratio of northern and southern source water, allowing for changes in the εNd endmember composition at the LGM. They found that the LGM authigenic εNd data were best supported by an increase in the northern source water endmember composition, without a substantial change in the relative northern source water–southern source water mixing fraction (Du et al. 2020). These studies collectively suggest nearly no change in AMOC geometry during the LGM, in direct conflict with the shoaling of NADW implied by $\delta^{13}C$ reconstructions.

Aside from the two most commonly cited circulation scenarios, namely shoaled upper cell or no structural change from the modern, there have been several other glacial circulation schemes that have been proposed in the literature, mostly in paleo-observational papers. These circulation configurations are attempts to satisfy a variety of (potentially conflicting) paleoproxy data, but have not necessarily been tested for their feasibility (i.e., by attempting to simulate these scenarios using physical models). One such scheme has a bifurcated glacial NADW (Howe et al. 2016; Pöppelmeier et al. 2020; Du et al. 2020)—an attempt to reconcile conflicting $\delta^{13}C$ and εNd data. In this hypothesis, both flavors of glacial NADW have negative εNd values, but the shallower version of GNADW is forms via open-ocean deep convection, imparting a heavy $\delta^{13}C$ composition, while the deeper version forms under sea ice with restricted air–sea gas exchange, and thus light $\delta^{13}C$. Coupled climate models of the LGM sometimes have large mixed-layer depths in both the Nordic seas and the region south of Iceland (Sherriff-Tadano et al. 2018), but these models do not appear to produce two types of NADW with very different densities. However, to our knowledge, no modeling studies have specifically tried to simulate a bifurcated glacial NADW, so its physical realism is unknown.

b. *Physical constraints on LGM circulation*

Larger Southern Ocean buoyancy loss is generally thought to cause shoaling of the AMOC, and larger diapycnal mixing is generally thought to cause deepening (as described in sections 2a and 2b). Idealized models have been fundamental to understanding the key processes that set AMOC depth, and they generally point to modest shoaling of the AMOC in the South Atlantic at the LGM (e.g., Nadeau and Jansen 2020; Baker et al. 2021). However, ultimately they cannot tell us whether increased buoyancy loss or increased diapycnal mixing is the most important effect at the LGM, because they do not represent the full complexity of the ocean system. Thus, we turn to more complex simulations to assess how the AMOC circulation may have changed at the LGM.

Models forced with glacial boundary conditions as part of PMIP do not produce consistent responses in terms of glacial overturning strength or the depth of the boundary between the upper and lower cells in the Atlantic (Otto-Bliesner et al. 2007; Weber et al. 2007; Muglia et al. 2018). As shown in Fig. S2, some PMIP simulations produce a deeper AMOC, some a shallower AMOC, and some no change in the depth of the AMOC. Marzocchi and Jansen (2017) attribute a deep AMOC in some of the PMIP simulations to insufficient sea ice formation, which causes less deep ocean stratification in these models. However, even assimilating proxy observations of LGM surface temperature does not guarantee that the AMOC will shoal (Amrhein et al. 2018). From physical models of the LGM ocean circulation that do not include geochemical tracers, it is difficult to rule out shoaling, no-change, or deepening circulation scenarios. These models are a useful starting point for understanding how different ocean circulations impact ocean tracer distributions, as discussed in section 1.

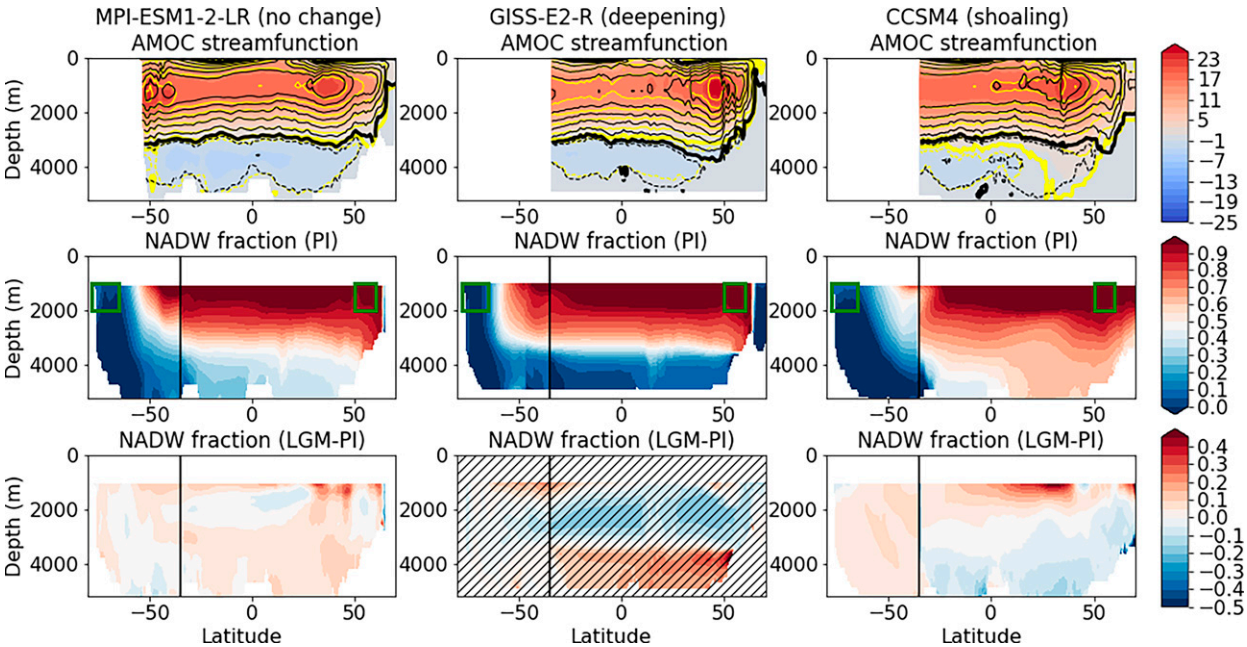

FIG. 3. (top) AMOC streamfunction in three climate models for preindustrial (yellow contours and background shading) and LGM (black contours) simulations. (middle) The thick contour highlights the 0.2-Sv streamline and can be thought of as the bottom edge of the upper cell. NADW fraction during the preindustrial (PI) simulation, estimated from temperature and using endpoints highlighted by the green rectangles. (bottom) NADW fraction during the LGM simulation minus NADW fraction during the preindustrial simulation, estimated from temperature and using endpoints highlighted by the green rectangles. The second panel in the bottom row is hatched because the GISS model was not run for long enough at the LGM for the deep ocean to reach equilibrium. The black vertical line indicates the latitude that separates the Atlantic from the Southern Ocean: north of this line, the zonal mean is taken over the Atlantic basin and south of this line the zonal mean is taken over the whole zonal extent of the domain. The Gulf of Mexico and Caribbean Seas are excluded from the zonal mean of CCSM NADW fraction. The MPI model run (Mauritsen et al. 2019; Müller et al. 2018) is part of the PMIP4 dataset (Kageyama et al. 2017), and the preindustrial CCSM (Gent et al. 2011) and GISS model (Schmidt et al. 2014) runs are part of the CMIP5 dataset. The LGM CCSM data are from the same runs used by Brady et al. (2013).

There is mounting evidence for increased diapycnal mixing at the LGM. Reduced sea level at the LGM (see section 2b) probably reduced tidal dissipation on continental shelves and caused more tidal energy to be dissipated in the deep ocean (Arbic et al. 2004; Egbert et al. 2004; Griffiths and Peltier 2009; Green 2010; Wilmes et al. 2019). Studies by Schmittner et al. (2015) and Wilmes et al. (2019) found that changes in tidal energy dissipation dominate over changes in ocean stratification, and tidally induced mixing affects diapycnal diffusivity most strongly in the North Atlantic below 2000 m, causing the upper cell to extend to 5000 m. In Wilmes et al.'s (2019) simulations with realistic tidally induced mixing, the upper cell only deepens by about 500 m north of 20°N and shows little change south of 20°N. A deeper AMOC in the North Atlantic is not completely ruled out by the observational record: more research is needed to explore this possibility.

SOURCES OF UNCERTAINTY IN OUR PHYSICAL UNDERSTANDING

The strength of diapycnal mixing in the global ocean is not well constrained either today or at the LGM. Vertical variations in the diapycnal diffusivity may lead to significant exchange between the upper and abyssal cells (Mashayek et al. 2017; Jones and Abernathey 2021). This transport may not be visible in the zonally integrated streamfunction, because downward transport in the interior may be cancelled by upward transport close to the ocean boundaries (Callies and Ferrari 2018), but it is likely to transport tracer between the upper and abyssal ocean. Hence, it is not clear how much a cell separation in the zonal mean streamfunction [as predicted by Ferrari et al. (2014)] would influence deep ocean tracer distributions. In this section, we explore how the tracer distributions in Fig. 3 may be impacted by mean ocean circulation and by other factors including diapycnal mixing.

Most PMIP models do not simulate the distribution of relevant paleo-oceanographic tracers like δ^{13}C and εNd, or even passive tracers for water masses like NADW and AABW. In Fig. 3, we attempt to estimate the fraction of deep Atlantic water that originated in the North Atlantic in three models based on the temperature distribution in these models. We chose to use temperature rather than salinity because the salinity of AABW and NADW were very similar in some of the LGM simulations. The results shown here are qualitatively very similar if salinity is chosen rather than temperature (as shown in Fig. S3).

The MPI and GISS models have similar preindustrial AMOC streamfunctions, in which the upper cell extends to

around 2500-m depth from 25°N to 25°S. However, the MPI model has significantly more NADW in the deep ocean. The differences in deep NADW concentration are most likely caused by the differences in ocean mixing between models, or perhaps differences in the zonal structure of the circulation. Changes in ocean mixing between the LGM and today are of similar magnitude as differences in modern mixing between different models (not shown). Thus ocean mixing changes could be *as important* as changes in circulation structure for ocean tracer distributions. CCSM4's preindustrial AMOC streamfunction extends to 5000 m in the North Atlantic at 30°N, and CCSM4 has much more NADW in the deep Atlantic than the other two simulations.

We repeated this analysis to find the concentration of NADW in the last century of the LGM simulations for each of these models. In the MPI model, which was run for 2300 years (starting from a previous LGM simulation), the MOC streamfunction does not change much between the LGM and preindustrial times, but there is slightly more NADW in the deep ocean at the LGM, highlighting that changing mixing processes may be important. We chose an extended LGM simulation of CCSM4 (Brady et al. 2013) that was run for 1600 years [for more details, see the supplementary information of Marzocchi and Jansen (2017)]. In CCSM4, the upper cell shoals at the LGM, and the NADW concentration in the deep ocean reduces as a result of this shoaling.

We chose the MPI and CCSM4 models partially because they had long LGM simulations: the MPI model was run for 2300 years (ensemble r1i1p1f1 in the CMIP6 archive; Mauritsen et al. 2019) and CCSM4 was run for 1600 years (Brady et al. 2013). The GISS model was only run for 300 years (ensemble r1i1p151 in the CMIP 5 archive; Schmidt et al. 2014), which is not long enough for water that was ventilated at the surface at the beginning of the simulation to reach the deep ocean (greater than 500 years in the deep tropical Atlantic; Khatiwala et al. 2012). Hence, in the GISS model we cannot find the NADW concentration in the deep ocean with any confidence. The LGM simulations from many models are not very long and it is likely that tracers in the deep ocean are not in equilibrium. If these simulations were run for at least 1500 years, it would most likely be possible to analyze how changes in ocean circulation impact deep ocean tracer distributions in these LGM simulations. Alternatively, the transport matrix, a mathematical operator that describes the motion of ocean tracers, could be calculated from short PMIP simulations of the LGM, and the transport matrix could then be used to integrate the tracer distribution forward in time until it reaches equilibrium (see, e.g., Bardin et al. 2014; Zanna et al. 2019; John et al. 2020; Chamberlain et al. 2019). It would also be useful if more model fields, such as vertical and lateral diffusivity, were saved and made available. Longer runs and more variables (and funding for these things) are needed for coupled climate models to be used to their full potential in understanding the LGM ocean.

It is still unclear how much diapycnal mixing or isopycnal mixing changed at the LGM. Along with the work of Wilmes et al. (2019) and Jones and Abernathey (2019), these experiments suggest that diapycnal mixing may have had a first-order effect on NADW distributions at the LGM. Jones and Abernathey (2019) also highlight the importance of isopycnal mixing, but conclude that changes in isopycnal mixing likely have only a modest effect on large scales. Further research on how ocean mixing and ocean tracer advection interact to produce large-scale tracer distributions is needed to fully quantify the uncertainties associated with these quantities.

A further source of uncertainty is that we do not know the formation sites for NADW at the LGM. Coarse-resolution models often overemphasize the Labrador Sea as a location for deep-water formation (Heuzé 2017), which may cause bias in the location of endmembers in LGM ocean simulations. New observations from the Overturning in the Subpolar North Atlantic Program (OSNAP; Lozier et al. 2017) array will be helpful for improving the representation of deep-water formation in this area. Without further information, it is difficult to assess whether deep water from two different northern-source locations might be present in NADW at the LGM.

c. *Beyond tracer sections*

As discussed in section 1, the distribution of tracers like εNd and $\delta^{13}C_{AS}$ in the deep ocean do not give direct information about the AMOC streamfunction. Alternate methods of looking at the relationship between ocean tracer concentrations, ocean mixing, and ocean circulation are sorely needed in order to extract the information stored in paleo-oceanographic observations.

One alternate way of examining ocean tracer distributions is to look at tracer–tracer cross plots (e.g., Hines et al. 2019) rather than tracer sections. When binary mixing occurs between two water masses, conservative tracers should plot linearly on a tracer–tracer plot (a common oceanographic example of this is a temperature–salinity diagram). By comparing the relationship between tracers in the modern ocean with their reconstructed relationship for the glacial ocean, we can deduce whether water mass endmembers changed significantly between these two periods.

We have compiled and merged datasets of benthic $\delta^{13}C_{DIC}$, $\delta^{13}C_{AS}$, and εNd for the LGM Atlantic below 2000 m (Fig. 4), where reconstructions of glacial Atlantic water mass geometry based on these proxies diverge significantly (Figs. 2d–f). In particular, $\delta^{13}C_{AS}$ is conservative by definition, and εNd is thought to be largely conservative in the interior Atlantic (Du et al. 2020)—any shifts in the relationships between these proxies are likely driven by changing endmembers.

There are few locations with collocated LGM $\delta^{13}C_{AS}$ and εNd reconstructions (Fig. 4a). However, the few observations available show a striking shift in the southern-source $\delta^{13}C_{AS}$ endmember during the LGM compared to present, with AABW shifted toward significantly lighter values than any observed in the modern Atlantic (Fig. 4a). In fact, the *directionality* of the $\delta^{13}C_{AS}$–εNd relationship for the LGM is completely reversed during the LGM, with AABW becoming isotopically lighter in $\delta^{13}C_{AS}$ than NADW. Since AABW subducts from the surface at the freezing point in the modern ocean, it is unlikely that colder AABW temperatures during the LGM could explain the lower $\delta^{13}C_{AS}$. Similarly, since AABW is isotopically lighter than NADW during the LGM, this signal must be primary, and not

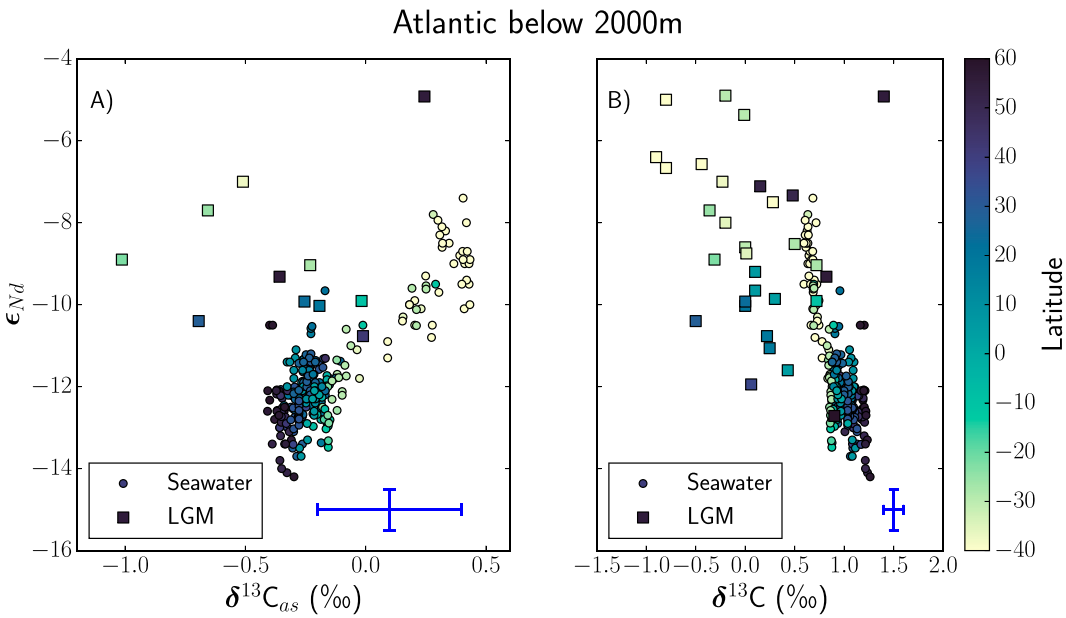

FIG. 4. Tracer–tracer plots for modern seawater (dots) and reconstructed values for the LGM (squares): (a) εNd and $\delta^{13}C_{AS}$ and (b) εNd and $\delta^{13}C_{DIC}$. The data source for LGM benthic $\delta^{13}C_{AS}$ and $\delta^{13}C$ is Oppo et al. (2018), and for LGM authigenic εNd the data source is Du et al. (2020). Seawater data for εNd also come from the compilation of Du et al. (2020). For seawater data points, we once again used the Eide et al. (2017) $\delta^{13}C$ climatology, and combined it with the World Ocean Atlas phosphate climatology to determine $\delta^{13}C_{AS}$ using Eq. (7). For each seawater εNd measurement in the Atlantic Basin below 2000 m, we then extracted $\delta^{13}C$ and $\delta^{13}C_{AS}$ values from the nearest latitude–longitude–depth grid cell. Blue lines at the bottom of the plots display representative uncertainties due to random errors associated with measurements involved in the respective proxies, but do not include possible systematic uncertainties associated with diagenetic influences on the proxies, or calibrations for the determination of derived parameters (e.g., the conversion of Cd/Ca and $\delta^{13}C$ to $\delta^{13}C_{AS}$).

due to variable entrainment with subsurface NADW. Instead, this signal must be driven by decreased air–sea equilibration during the LGM and/or decreased net sea to air CO_2 flux. This reversal in the $\delta^{13}C_{AS}$ gradient at the LGM has been previously documented (Marchitto and Broecker 2006; Oppo et al. 2018; Gebbie 2014) and even simulated in a model (Menviel et al. 2020). It is generally attributed to reduced air–sea gas exchange, possibly by increased sea ice cover, in the Southern Ocean and colder temperatures in the North Atlantic.

Another way of using paleoceanographic tracers is to use them as direct physical constraints on circulation. The oxygen isotopic composition of seawater, $\delta^{18}O$, is a function of its temperature and salinity, as is density. While $\delta^{18}O$ is not a proxy for density per se, this physical relationship is still powerful. Lund et al. (2011) observed shifts in the difference between LGM and Holocene $\delta^{18}O$ values at approximately 2000-m water depth in two depth profiles from the Brazil Margin (30°S) and Blake Ridge (30°N) in the Atlantic. Motivated by this observation, Lund et al. (2011) constructed a two-dimensional tracer budget for the Atlantic across a surface that marks the boundary between a southern sourced water mass (i.e., AABW) and a northern sourced water mass (i.e., NADW). The gradient of a tracer across this surface is proportional to the ratio of the overturning strength of the deep water mass divided by the vertical diffusivity across the surface (Ψ/κ). Accounting for changes in the surface area of that water mass boundary, the authors calculate that Ψ/κ was larger at the LGM compared to today. This could be achieved either by decreasing the vertical diffusivity (κ) or increasing the deep overturning circulation (Ψ). Lund et al. (2011) conclude that the most likely explanation for the change in $\delta^{18}O$ distribution is that the interface between the abyssal and upper cells of the MOC shoaled, causing a decrease in κ across this interface.

When considering the difficulties in interpreting tracer sections in terms of LGM water mass changes we discussed in section 4b., the results of Lund et al. (2011) are perhaps the most straightforward approach showing evidence for shoaled NADW during the LGM. Ideally their approach could be applied to the entirety of the LGM Atlantic basin. Unfortunately, as the authors discuss, interlaboratory offsets in $\delta^{18}O$ of roughly 0.3‰ are on the same order as the vertical LGM $\delta^{18}O$ kink. Thus, their analysis cannot yet be extended to additional locations or to a compilation of Atlantic LGM benthic $\delta^{18}O$. Distributed time slice benthic $\delta^{18}O$ across several depth transects from a single laboratory would be an extremely valuable step toward confirming (or ruling out) the ubiquity of LGM Atlantic Ψ/κ changes. Recent work by Wilmes et al. (2021) shows that a large increase in the vertical diffusivity at all depths is not consistent with Lund's

result even for a shallow LGM overturning circulation. This highlights the need for more observational evidence to characterize whether Ψ/κ has increased or decreased since the LGM. Such evidence could be useful for understanding both large-scale circulation and vertical mixing in the past.

Finally, from the modeling side, several studies (e.g., Brovkin et al. 2007; Tagliabue et al. 2009; Bouttes et al. 2011; Menviel et al. 2017; Muglia et al. 2018; Gu et al. 2020; Menviel et al. 2020; Muglia and Schmittner 2021; Wilmes et al. 2021) have included geochemical tracers into LGM simulations in order to directly compare simulated distributions with proxy measurements (given known circulation configurations by definition). Recognizing the computational challenges of incorporating these tracers, it is particularly beneficial to include multiple tracers (e.g., Gu et al. 2020; Muglia and Schmittner 2021). This will allow for more unique insights from model output, such as the construction of tracer–tracer plots for diagnosing proxy behavior in the model—the value of which in observational data is discussed earlier in this section.

5. Conclusions

This paper highlights that neither observations nor models provide clear evidence of whether the AMOC shoaled at the LGM. The εNd records indicate that NADW reached the deep Atlantic at the LGM, while the δ^{13}C records suggest that NADW was confined to the top 1500 m or so. Models also disagree about whether the AMOC shoaled at the LGM, and many models only represent the circulation, temperature, and salinity, so they provide limited information about past tracer distributions. Models can be tuned to give a range of answers, and while idealized models are very valuable for understanding the processes that set the depth of the AMOC, it is important to understand that existing models only scratch the surface of the possible range of mixing parameters that may have occurred at the LGM.

In light of this continued uncertainty about the state of the ocean circulation at the LGM, we conclude this paper with some suggestions for how to clarify the science, while giving proper weight to the huge complexity of inferring ocean circulation from limited ocean tracer observations.

We have shown in this paper that collocated records of conservative and quasi-conservative tracers allow for the determination of mixing relationships between water masses, as well as diagnosis of changing proxy endmembers, via tracer–tracer plots. These types of analyses are in their nascent stages, and hold considerable promise for future reconstructions of water mass characteristics. One way to clarify existing discrepancies between εNd and $\delta^{13}C_{AS}$ would be to greatly expand the number of collocated εNd and $\delta^{13}C_{AS}$ measurements during the LGM and Holocene, via a time slice approach. Further, these cross-plot analyses could be expanded to include non-conservative tracers (e.g., $\Delta\delta^{13}C_{DIC}$ for bottom water oxygen concentrations, B/Ca for carbonate ions, etc.).

Some paleo data–model comparison has been done to test the validity of PMIP and PMIP-like models (e.g., Brovkin et al. 2007; Tagliabue et al. 2009; Bouttes et al. 2011; Menviel et al. 2017; Muglia et al. 2018; Gu et al. 2020; Menviel et al. 2020; Muglia and Schmittner 2021; Wilmes et al. 2021), but the majority of these studies use only δ^{13}C or δ^{13}C and radiocarbon as a paleoceanographic tracer and all of them focus on a single model. Given that the different PMIP models have naturally resulted in variable glacial circulations, it would be informative to see a model–data comparison across all these models, comparing not only δ^{13}C data but also proxies such as εNd and $\delta^{13}C_{AS}$, and NADW concentration estimates based on temperature and salinity distributions. We acknowledge that implementing such a large number of tracers in all the PMIP models may not be the most efficient use of time, so one potential solution is to produce transport matrices for these models in order to generate proxy distributions using an offline tool like the Ocean Circulation Inverse Model (OCIM) (DeVries and Primeau 2011).

Another challenge in this problem is the huge number of parameters that control ocean tracer distributions, including the 3D distribution of mixing, the boundary conditions for each of the tracers, and possible changes in circulation. Idealized models are useful for exploring a wide range of parameters at low computational cost. In the future, including tracers for water masses and their ages in idealized modeling studies will allow for their results to be more easily interpreted from an observational standpoint.

By working together, observationalists and modelers can better select sampling locations that will provide maximum information content. Selection of these locations should be informed by models (especially those that simulate tracers), but also take into account the expertise of paleoceanographers, who know best whether proxy data can be obtained at a specific location.

In conclusion, recent research has shown that paleo-tracers contain a wealth of information about surface and mixing processes, in addition to information about the large-scale ocean circulation. This highlights an opportunity to increase our understanding of past ocean states beyond what was previously assumed. Ultimately, this approach will result in a deeper, more complete understanding of LGM Atlantic circulation changes.

Acknowledgments. The authors thank Esther Brady, who provided data from the extended CCSM model run, together with Alan Seltzer, Kassandra Costa, Shantong Sun, and Andrew Thompson, who all read the manuscript and provided valuable feedback. Two anonymous reviewers and Andreas Schmittner contributed thorough and insightful reviews that improved the paper. S.K.H. was supported by the Investment in Science Fund at WHOI and the John E. and Anne W. Sawyer Endowed Fund in Support of Scientific Staff. F.J.P. was supported by a Stanback Postdoctoral Fellowship at Caltech.

Data availability statement. We acknowledge the World Climate Research Programme's Working Group on Coupled Modelling, which is responsible for CMIP, and we thank the climate modeling groups (MPI, NASA GISS and CESM) for producing and making available their model output, the Earth System Grid Federation (ESGF) for archiving the data and providing access, and the multiple funding agencies that

support CMIP and ESGF. The CESM project is supported by the National Science Foundation and the Office of Science (BER) of the U.S. Department of Energy. NCAR is sponsored by the National Science Foundation. Computing resources were provided by the Climate Simulation Laboratory at the NCAR Computational and Information Systems Laboratory (CISL), sponsored by the National Science Foundation and other agencies.

The MPI model data used here can be found at https://esgf-node.llnl.gov/search/cmip6/ and the GISS data can be found at https://esgf-node.llnl.gov/search/cmip5/. The preindustrial run of CCSM4 is available at https://www.earthsystemgrid.org/search.html?Project=CMIP5. The LGM CCSM4 data used in this manuscript are from the extended run described in Brady et al. (2013). We regret that these data are not publicly available at this time, but they are present on the glade file system. The data sources in Figs. 2 and 4 are as follows. The modern seawater carbon isotope data is from Eide et al. (2017) (https://doi.pangaea.de/10.1594/PANGAEA.871962). Modern and LGM εNd data are from the supplementary material of Du et al. (2020). LGM δ^{13}C and $\delta^{13}C_{AS}$ are from the compiled data in the supplementary material of Oppo et al. (2018).

REFERENCES

Abernathey, R., and D. Ferreira, 2015: Southern Ocean isopycnal mixing and ventilation changes driven by winds. *Geophys. Res. Lett.*, **42**, 10 357–10 365, https://doi.org/10.1002/2015GL066238.

——, I. Cerovecki, P. R. Holland, E. Newsom, M. Mazloff, and L. D. Talley, 2016: Water-mass transformation by sea ice in the upper branch of the Southern Ocean overturning. *Nat. Geosci.*, **9**, 596–601, https://doi.org/10.1038/ngeo2749.

Adkins, J. F., 2013: The role of deep ocean circulation in setting glacial climates. *Paleoceanogr. Paleoclimatol.*, **28**, 539–561, https://doi.org/10.1002/palo.20046.

Amrhein, D. E., C. Wunsch, O. Marchal, and G. Forget, 2018: A global glacial ocean state estimate constrained by upper-ocean temperature proxies. *J. Climate*, **31**, 8059–8079, https://doi.org/10.1175/JCLI-D-17-0769.1.

Arbic, B. K., D. R. MacAyeal, J. X. Mitrovica, and G. A. Milne, 2004: Ocean tides and Heinrich events. *Nature*, **432**, 460, https://doi.org/10.1038/432460a.

Baker, J. A., A. J. Watson, and G. K. Vallis, 2020: Meridional overturning circulation in a multibasin model. Part I: Dependence on Southern Ocean buoyancy forcing. *J. Phys. Oceanogr.*, **50**, 1159–1178, https://doi.org/10.1175/JPO-D-19-0135.1.

——, ——, and ——, 2021: Meridional overturning circulation in a multibasin model. Part II: Sensitivity to diffusivity and wind in warm and cool climates. *J. Phys. Oceanogr.*, **51**, 1813–1828, https://doi.org/10.1175/JPO-D-20-0121.1.

Bardin, A., F. Primeau, and K. Lindsay, 2014: An offline implicit solver for simulating prebomb radiocarbon. *Ocean Modell.*, **73**, 45–58, https://doi.org/10.1016/j.ocemod.2013.09.008.

Blaser, P., and Coauthors, 2019: The resilience and sensitivity of northeast Atlantic deep water εNd to overprinting by detrital fluxes over the past 30,000 years. *Geochim. Cosmochim. Acta*, **245**, 79–97, https://doi.org/10.1016/j.gca.2018.10.018.

Bouttes, N., D. Paillard, D. M. Roche, V. Brovkin, and L. Bopp, 2011: Last Glacial Maximum CO_2 and δ^{13}C successfully reconciled. *Geophys. Res. Lett.*, **38**, L02705, https://doi.org/10.1029/2010GL044499.

Bower, A., and Coauthors, 2019: Lagrangian views of the pathways of the Atlantic meridional overturning circulation. *J. Geophys. Res. Oceans*, **124**, 5313–5335, https://doi.org/10.1029/2019JC015014.

Boyle, E. A., 1988: Cadmium: Chemical tracer of deepwater paleoceanography. *Paleoceanogr. Paleoclimatol.*, **3**, 471–489, https://doi.org/10.1029/PA003i004p00471.

Brady, E. C., B. L. Otto-Bliesner, J. E. Kay, and N. Rosenbloom, 2013: Sensitivity to glacial forcing in the CCSM4. *J. Climate*, **26**, 1901–1925, https://doi.org/10.1175/JCLI-D-11-00416.1.

Broecker, W. S., and Coauthors, 1998: How much deep water is formed in the Southern Ocean? *J. Geophys. Res.*, **103**, 15 833–15 843, https://doi.org/10.1029/98JC00248.

Brovkin, V., A. Ganopolski, D. Archer, and S. Rahmstorf, 2007: Lowering of glacial atmospheric CO_2 in response to changes in oceanic circulation and marine biogeochemistry. *Paleoceanogr. Paleoclimatol.*, **22**, PA4202, https://doi.org/10.1029/2006PA001380.

Burke, A., A. L. Stewart, J. F. Adkins, R. Ferrari, M. F. Jansen, and A. F. Thompson, 2015: The glacial mid-depth radiocarbon bulge and its implications for the overturning circulation. *Paleoceanogr. Paleoclimatol.*, **30**, 1021–1039, https://doi.org/10.1002/2015PA002778.

Callies, J., and R. Ferrari, 2018: Dynamics of an abyssal circulation driven by bottom-intensified mixing on slopes. *J. Phys. Oceanogr.*, **48**, 1257–1282, https://doi.org/10.1175/JPO-D-17-0125.1.

Chamberlain, M. A., R. J. Matear, M. Holzer, D. Bi, and S. J. Marsland, 2019: Transport matrices from standard ocean-model output and quantifying circulation response to climate change. *Ocean Modell.*, **135**, 1–13, https://doi.org/10.1016/j.ocemod.2019.01.005.

Charles, C. D., J. D. Wright, and R. G. Fairbanks, 1993: Thermodynamic influences on the marine carbon isotope record. *Paleoceanogr. Paleoclimatol.*, **8**, 691–697, https://doi.org/10.1029/93PA01803.

Chassignet, E. P., and Coauthors, 2020: Impact of horizontal resolution on global ocean–sea ice model simulations based on the experimental protocols of the Ocean Model Intercomparison Project phase 2 (OMIP-2). *Geosci. Model Dev.*, **13**, 4595–4637, https://doi.org/10.5194/gmd-13-4595-2020.

Curry, W. B., and D. W. Oppo, 2005: Glacial water mass geometry and the distribution of δ^{13}C of ΣCO_2 in the western Atlantic Ocean. *Paleoceanogr. Paleoclimatol.*, **20**, PA1017, https://doi.org/10.1029/2004PA001021.

DeVries, T., and F. Primeau, 2011: Dynamically and observationally constrained estimates of water-mass distributions and ages in the global ocean. *J. Phys. Oceanogr.*, **41**, 2381–2401, https://doi.org/10.1175/JPO-D-10-05011.1.

Du, J., B. A. Haley, and A. C. Mix, 2020: Evolution of the global overturning circulation since the Last Glacial Maximum based on marine authigenic neodymium isotopes. *Quat. Sci. Rev.*, **241**, 106396, https://doi.org/10.1016/j.quascirev.2020.106396.

Duplessy, J.-C., N. J. Shackleton, R. G. Fairbanks, L. Labeyrie, D. Oppo, and N. Kallel, 1988: Deep water source variations during the last climatic cycle and their impact on the global deep water circulation. *Paleoceanogr. Paleoclimatol.*, **3**, 343–360, https://doi.org/10.1029/PA003i003p00343.

Egbert, G. D., R. D. Ray, and B. G. Bills, 2004: Numerical modeling of the global semidiurnal tide in the present day

and in the last glacial maximum. *J. Geophys. Res.*, **109**, C03003, https://doi.org/10.1029/2003JC001973.

Eide, M., A. Olsen, U. S. Ninnemann, and T. Johannessen, 2017: A global ocean climatology of preindustrial and modern ocean δ^{13}C. *Global Biogeochem. Cycles*, **31**, 515–534, https://doi.org/10.1002/2016GB005473.

Elderfield, H., and R. E. M. Rickaby, 2000: Oceanic Cd/P ratio and nutrient utilization in the glacial Southern Ocean. *Nature*, **405**, 305–310, https://doi.org/10.1038/35012507.

Ferrari, R., M. F. Jansen, J. F. Adkins, A. Burke, A. L. Stewart, and A. F. Thompson, 2014: Antarctic sea ice control on ocean circulation in present and glacial climates. *Proc. Natl. Acad. Sci. USA*, **111**, 8753–8758, https://doi.org/10.1073/pnas.1323922111.

——, A. Mashayek, T. J. McDougall, M. Nikurashin, and J.-M. Campin, 2016: Turning ocean mixing upside down. *J. Phys. Oceanogr.*, **46**, 2239–2261, https://doi.org/10.1175/JPO-D-15-0244.1.

——, L.-P. Nadeau, D. P. Marshall, L. C. Allison, and H. L. Johnson, 2017: A model of the ocean overturning circulation with two closed basins and a reentrant channel. *J. Phys. Oceanogr.*, **47**, 2887–2906, https://doi.org/10.1175/JPO-D-16-0223.1.

Galbraith, E., and C. de Lavergne, 2018: Response of a comprehensive climate model to a broad range of external forcings: Relevance for deep ocean ventilation and the development of late Cenozoic ice ages. *Climate Dyn.*, **52**, 653–679, https://doi.org/10.1007/s00382-018-4157-8.

Gebbie, G., 2014: How much did glacial North Atlantic Water shoal? *Paleoceanogr. Paleoclimatol.*, **29**, 190–209, https://doi.org/10.1002/2013PA002557.

Gent, P. R., 2016: Effects of Southern Hemisphere wind changes on the meridional overturning circulation in ocean models. *Ann. Rev. Mar. Sci.*, **8**, 79–94, https://doi.org/10.1146/annurev-marine-122414-033929.

——, and Coauthors, 2011: The Community Climate System Model version 4. *J. Climate*, **24**, 4973–4991, https://doi.org/10.1175/2011JCLI4083.1.

Gersonde, R., X. Crosta, A. Abelmann, and L. K. Armand, 2005: Sea-surface temperature and sea ice distribution of the Southern Ocean at the EPILOG Last Glacial Maximum—A circum-Antarctic view based on siliceous microfossil records. *Quat. Sci. Rev.*, **24**, 869–896, https://doi.org/10.1016/j.quascirev.2004.07.015.

Gherardi, J., L. Labeyrie, S. Nave, R. Francois, J. F. McManus, and E. Cortijo, 2009: Glacial-interglacial circulation changes inferred from ^{231}Pa/^{230}Th sedimentary record in the North Atlantic region. *Paleoceanogr. Paleoclimatol.*, **24**, PA2204, https://doi.org/10.1029/2008PA001696.

Goldstein, S., and S. R. Hemming, 2003: Long-lived isotopic tracers in oceanography, paleoceanography, and ice-sheet dynamics. *Treatise on Geochemistry*, H. Elderfield and K. K. Turekian, Elsevier, 453–489, https://doi.org/10.1016/B0-08-043751-6/06179-X

Gottschalk, J., N. V. Riveiros, C. Waelbroeck, L. C. Skinner, E. Michel, J.-C. Duplessy, D. Hodell, and A. Mackensen, 2016: Carbon isotope offsets between benthic foraminifer species of the genus *Cibicides* (Cibicidoides) in the glacial sub-Antarctic Atlantic. *Paleoceanogr. Paleoclimatol.*, **31**, 1583–1602, https://doi.org/10.1002/2016PA003029.

——, and Coauthors, 2019: Mechanisms of millennial-scale atmospheric CO_2 change in numerical model simulations. *Quat. Sci. Rev.*, **220**, 30–74, https://doi.org/10.1016/j.quascirev.2019.05.013.

Green, J. A. M., 2010: Ocean tides and resonance. *Ocean Dyn.*, **60**, 1243–1253, https://doi.org/10.1007/s10236-010-0331-1.

Griffiths, S. D., and W. R. Peltier, 2009: Modeling of polar ocean tides at the last glacial maximum: Amplification, sensitivity, and climatological implications. *J. Climate*, **22**, 2905–2924, https://doi.org/10.1175/2008JCLI2540.1.

Gu, S., Z. Liu, D. W. Oppo, J. Lynch-Stieglitz, A. Jahn, J. Zhang, and L. Wu, 2020: Assessing the potential capability of reconstructing glacial Atlantic water masses and AMOC using multiple proxies in CESM. *Earth Planet. Sci. Lett.*, **541**, 116294, https://doi.org/10.1016/j.epsl.2020.116294.

Haley, B. A., J. Du, A. N. Abbott, and J. McManus, 2017: The impact of benthic processes on rare earth element and neodymium isotope distributions in the oceans. *Front. Mar. Sci.*, **4**, 426, https://doi.org/10.3389/fmars.2017.00426.

Heuzé, C., 2017: North Atlantic deep water formation and AMOC in CMIP5 models. *Ocean Sci.*, **13**, 609–622, https://doi.org/10.5194/os-13-609-2017.

Hines, S. K. V., A. F. Thompson, and J. F. Adkins, 2019: The role of the Southern Ocean in abrupt transitions and hysteresis in glacial ocean circulation. *Paleoceanogr. Paleoclimatol.*, **34**, 490–510, https://doi.org/10.1029/2018PA003415.

Ho, S. L., and Coauthors, 2012: Sea surface temperature variability in the Pacific sector of the Southern Ocean over the past 700 kyr. *Paleoceanogr. Paleoclimatol.*, **27**, PA4202, https://doi.org/10.1029/2012PA002317.

Howe, J. N. W., A. M. Piotrowski, T. L. Noble, S. Mulitza, C. M. Chiessi, and G. Bayon, 2016: North Atlantic Deep Water production during the Last Glacial Maximum. *Nat. Commun.*, **7**, 11765, https://doi.org/10.1038/ncomms11765.

Jacobsen, S. B., and G. J. Wasserburg, 1980: Sm-Nd isotopic evolution of chondrites. *Earth Planet. Sci. Lett.*, **50**, 139–155, https://doi.org/10.1016/0012-821X(80)90125-9.

Jansen, M. F., 2017: Glacial ocean circulation and stratification explained by reduced atmospheric temperature. *Proc. Natl. Acad. Sci. USA*, **114**, 45–50, https://doi.org/10.1073/pnas.1610438113.

——, and L.-P. Nadeau, 2016: The effect of Southern Ocean surface buoyancy loss on the deep-ocean circulation and stratification. *J. Phys. Oceanogr.*, **46**, 3455–3470, https://doi.org/10.1175/JPO-D-16-0084.1.

Jeandel, C., 2016: Overview of the mechanisms that could explain the 'boundary exchange' at the land–ocean contact. *Philos. Trans. Roy. Soc.*, **A374**, 20150287, https://doi.org/10.1098/rsta.2015.0287.

John, S. G., and Coauthors, 2020: AWESOME OCIM: A simple, flexible, and powerful tool for modeling elemental cycling in the oceans. *Chem. Geol.*, **533**, 119403,. https://doi.org/10.1016/j.chemgeo.2019.119403.

Johnson, H. L., P. Cessi, D. P. Marshall, F. Schloesser, and M. A. Spall, 2019: Recent contributions of theory to our understanding of the Atlantic meridional overturning circulation. *J. Geophys. Res. Oceans*, **124**, 5376–5399, https://doi.org/10.1029/2019JC015330.

Jones, C. S., and P. Cessi, 2016: Interbasin transport of the meridional overturning circulation. *J. Phys. Oceanogr.*, **46**, 1157–1169, https://doi.org/10.1175/JPO-D-15-0197.1.

——, and R. P. Abernathey, 2019: Isopycnal mixing controls deep ocean ventilation. *Geophys. Res. Lett.*, **46**, 13 144–13 151, https://doi.org/10.1029/2019GL085208.

——, and ——, 2021: Modeling water-mass distributions in the modern and LGM ocean: Circulation change and isopycnal

and diapycnal mixing. *J. Phys. Oceanogr.*, **51**, 1523–1538, https://doi.org/10.1175/JPO-D-20-0204.1.

Kageyama, M., and Coauthors, 2017: The PMIP4 contribution to CMIP6—Part 4: Scientific objectives and experimental design of the PMIP4-CMIP6 Last Glacial Maximum experiments and PMIP4 sensitivity experiments. *Geosci. Model Dev.*, **10**, 4035–4055, https://doi.org/10.5194/gmd-10-4035-2017.

Key, R., and Coauthors, 2004: A global ocean carbon climatology: Results from Global Data Analysis Project (GLODAP). *Global Biogeochem. Cycles*, **18** (4), 1–23, https://doi.org/10.1029/2004GB002247.

Khatiwala, S., F. Primeau, and M. Holzer, 2012: Ventilation of the deep ocean constrained with tracer observations and implications for radiocarbon estimates of ideal mean age. *Earth Planet. Sci. Lett.*, **325–326**, 116–125, https://doi.org/10.1016/j.epsl.2012.01.038.

——, A. Schmittner, and J. Muglia, 2019: Air–sea disequilibrium enhances ocean carbon storage during glacial periods. *Sci. Adv.*, **5**, eaaw4981, https://doi.org/10.1126/sciadv.aaw4981.

Kim, J.-H., R. R. Schneider, S. Mulitza, and P. J. Müller, 2003: Reconstruction of SE trade-wind intensity based on sea-surface temperature gradients in the southeast Atlantic over the last 25 kyr. *Geophys. Res. Lett.*, **30**, 2144, https://doi.org/10.1029/2003GL017557.

Knox, F., and M. B. McElroy, 1984: Changes in atmospheric CO_2: Influence of the marine biota at high latitude. *J. Geophys. Res.*, **89**, 4629, https://doi.org/10.1029/JD089iD03p04629.

Kohfeld, K. E., R. M. Graham, A. M. de Boer, L. C. Sime, E. W. Wolff, C. Le Quéré, and L. Bopp, 2013: Southern Hemisphere westerly wind changes during the Last Glacial Maximum: Paleo-data synthesis. *Quat. Sci. Rev.*, **68**, 76–95, https://doi.org/10.1016/j.quascirev.2013.01.017.

Kwon, E. Y., M. P. Hain, D. M. Sigman, E. D. Galbraith, J. L. Sarmiento, and J. R. Toggweiler, 2012: North Atlantic ventilation of "southern-sourced" deep water in the glacial ocean. *Paleoceanogr. Paleoclimatol.*, **27**, PA2208, https://doi.org/10.1029/2011PA002211.

Lambelet, M., and Coauthors, 2016: Neodymium isotopic composition and concentration in the western North Atlantic Ocean: Results from the GEOTRACES GA02 section. *Geochim. Cosmochim. Acta*, **177**, 1–29, https://doi.org/10.1016/j.gca.2015.12.019.

Ledwell, J. R., E. T. Montgomery, K. L. Polzin, L. C. S. Laurent, R. W. Schmitt, and J. M. Toole, 2000: Evidence for enhanced mixing over rough topography in the abyssal ocean. *Nature*, **403**, 179–182, https://doi.org/10.1038/35003164.

Lin, P., and Coauthors, 2020: LICOM model datasets for the CMIP6 Ocean Model Intercomparison Project. *Adv. Atmos. Sci.*, **37**, 239–249, https://doi.org/10.1007/s00376-019-9208-5.

Lippold, J., Y. Luo, R. Francois, S. E. Allen, J. Gherardi, S. Pichat, B. Hickey, and H. Schulz, 2012: Strength and geometry of the glacial Atlantic meridional overturning circulation. *Nat. Geosci.*, **5**, 813–816, https://doi.org/10.1038/ngeo1608.

Lozier, M. S., and Coauthors, 2017: Overturning in the subpolar North Atlantic program: A new international ocean observing system. *Bull. Amer. Meteor. Soc.*, **98**, 737–752, https://doi.org/10.1175/BAMS-D-16-0057.1.

Lund, D. C., J. F. Adkins, and R. Ferrari, 2011: Abyssal Atlantic circulation during the Last Glacial Maximum: Constraining the ratio between transport and vertical mixing. *Paleoceanogr. Paleoclimatol.*, **26**, PA1213, https://doi.org/10.1029/2010PA001938.

Lynch-Stieglitz, J., and R. G. Fairbanks, 1994: A conservative tracer for glacial ocean circulation from carbon isotope and palaeo-nutrient measurements in benthic foraminifera. *Nature*, **369**, 308–310, https://doi.org/10.1038/369308a0.

——, T. F. Stocker, W. S. Broecker, and R. G. Fairbanks, 1995: The influence of air–sea exchange on the isotopic composition of oceanic carbon: Observations and modeling. *Global Biogeochem. Cycles*, **9**, 653–665, https://doi.org/10.1029/95GB02574.

Mackensen, A., 2012: Strong thermodynamic imprint on recent bottom-water and epibenthic $\delta^{13}C$ in the Weddell Sea revealed: Implications for glacial Southern Ocean ventilation. *Earth Planet. Sci. Lett.*, **317–318**, 20–26, https://doi.org/10.1016/j.epsl.2011.11.030.

——, H.-W. Hubberten, T. Bickert, G. Fischer, and D. K. Fütterer, 1993: The $\delta^{13}C$ in benthic foraminiferal tests of *Fontbotia wuellerstorfi* (Schwager) relative to the $\delta^{13}C$ of dissolved inorganic carbon in Southern Ocean deep water: Implications for glacial ocean circulation models. *Paleoceanogr. Paleoclimatol.*, **8**, 587–610, https://doi.org/10.1029/93PA01291.

Marchitto, T. M., and W. S. Broecker, 2006: Deep water mass geometry in the glacial Atlantic Ocean: A review of constraints from the paleonutrient proxy Cd/Ca. *Geochem. Geophys. Geosyst.*, **7**, Q12003, https://doi.org/10.1029/2006GC001323.

Marshall, J., and T. Radko, 2003: Residual-mean solutions for the Antarctic Circumpolar Current and its associated overturning circulation. *J. Phys. Oceanogr.*, **33**, 2341–2354, https://doi.org/10.1175/1520-0485(2003)033<2341:RSFTAC>2.0.CO;2.

——, and K. Speer, 2012: Closure of the meridional overturning circulation through Southern Ocean upwelling. *Nat. Geosci.*, **5**, 171–180, https://doi.org/10.1038/ngeo1391.

Marzocchi, A., and M. F. Jansen, 2017: Connecting Antarctic sea ice to deep-ocean circulation in modern and glacial climate simulations. *Geophys. Res. Lett.*, **44**, 6286–6295, https://doi.org/10.1002/2017GL073936.

Mashayek, A., H. Salehipour, D. Bouffard, C. Caulfield, R. Ferrari, M. Nikurashin, W. Peltier, and W. Smyth, 2017: Efficiency of turbulent mixing in the abyssal ocean circulation. *Geophys. Res. Lett.*, **44**, 6296–6306, https://doi.org/10.1002/2016GL072452.

Mauritsen, T., and Coauthors, 2019: Developments in the MPI-M Earth system model version 1.2 (MPI-ESM1.2) and its response to increasing CO_2. *J. Adv. Model. Earth Syst.*, **11**, 998–1038, https://doi.org/10.1029/2018MS001400.

McManus, J. F., R. Francois, J. M. Gherardi, L. D. Keigwin, and S. Brown-Leger, 2004: Collapse and rapid resumption of Atlantic meridional circulation linked to deglacial climate changes. *Nature*, **428**, 834–837, https://doi.org/10.1038/nature02494.

Menviel, L., J. Yu, F. Joos, A. Mouchet, K. J. Meissner, and M. H. England, 2017: Poorly ventilated deep ocean at the Last Glacial Maximum inferred from carbon isotopes: A data–model comparison study. *Paleoceanogr. Paleoclimatol.*, **32**, 2–17, https://doi.org/10.1002/2016PA003024.

——, P. Spence, L. C. Skinner, K. Tachikawa, T. Friedrich, L. Missiaen, and J. Yu, 2020: Enhanced mid-depth southward transport in the northeast Atlantic at the Last Glacial Maximum despite a weaker AMOC. *Paleoceanogr. Paleoclimatol.*, **35**, e2019PA003793, https://doi.org/10.1029/2019PA003793.

Middag, R., S. M. A. C. van Heuven, K. W. Bruland, and H. J. W. de Baar, 2018: The relationship between cadmium and phosphate in the Atlantic Ocean unravelled. *Earth*

Planet. Sci. Lett., **492**, 79–88, https://doi.org/10.1016/j.epsl.2018.03.046.

Miller, M. D., J. F. Adkins, D. Menemenlis, and M. P. Schodlok, 2012: The role of ocean cooling in setting Glacial Southern Source Bottom Water salinity. *Paleoceanogr. Paleoclimatol.*, **27**, PA3207, https://doi.org/10.1029/2012PA002297.

Muglia, J., and A. Schmittner, 2021: Carbon isotope constraints on glacial Atlantic meridional overturning: Strength vs depth. *Quat. Sci. Rev.*, **257**, 106844, https://doi.org/10.1016/j.quascirev.2021.106844.

——, L. C. Skinner, and A. Schmittner, 2018: Weak overturning circulation and high Southern Ocean nutrient utilization maximized glacial ocean carbon. *Earth Planet. Sci. Lett.*, **496**, 47–56, https://doi.org/10.1016/j.epsl.2018.05.038.

Müller, W. A., and Coauthors, 2018: A higher-resolution version of the Max Planck Institute Earth System Model (MPI-ESM1.2-hr). *J. Adv. Model. Earth Syst.*, **10**, 1383–1413, https://doi.org/10.1029/2017MS001217.

Nadeau, L.-P., and M. F. Jansen, 2020: Overturning circulation pathways in a two-basin ocean model. *J. Phys. Oceanogr.*, **50**, 2105–2122, https://doi.org/10.1175/JPO-D-20-0034.1.

——, R. Ferrari, and M. F. Jansen, 2019: Antarctic sea ice control on the depth of North Atlantic Deep Water. *J. Climate*, **32**, 2537–2551, https://doi.org/10.1175/JCLI-D-18-0519.1.

Oppo, D. W., G. Gebbie, K.-F. Huang, W. B. Curry, T. M. Marchitto, and K. R. Pietro, 2018: Data constraints on glacial Atlantic water mass geometry and properties. *Paleoceanogr. Paleoclimatol.*, **33**, 1013–1034, https://doi.org/10.1029/2018PA003408.

Otto-Bliesner, B. L., C. D. Hewitt, T. M. Marchitto, E. C. Brady, A. Abe-Ouchi, M. Crucifix, S. Murakami, and S. L. Weber, 2007: Last Glacial Maximum ocean thermohaline circulation: PMIP2 model intercomparisons and data constraints. *Geophys. Res. Lett.*, **34**, L12706, https://doi.org/10.1029/2007GL029475.

Pellichero, V., J.-B. Sallée, C. C. Chapman, and S. M. Downes, 2018: The southern ocean meridional overturning in the sea-ice sector is driven by freshwater fluxes. *Nat. Commun.*, **9**, 1789, https://doi.org/10.1038/s41467-018-04101-2.

Pena, L. D., and S. L. Goldstein, 2014: Thermohaline circulation crisis and impacts during the mid-Pleistocene transition. *Science*, **345**, 318–322, https://doi.org/10.1126/science.1249770.

Piotrowski, A. M., S. L. Goldstein, S. R. Hemming, and R. G. Fairbanks, 2004: Intensification and variability of ocean thermohaline circulation through the last deglaciation. *Earth Planet. Sci. Lett.*, **225**, 205–220, https://doi.org/10.1016/j.epsl.2004.06.002.

Polzin, K. L., J. M. Toole, J. R. Ledwell, and R. W. Schmitt, 1997: Spatial variability of turbulent mixing in the abyssal ocean. *Science*, **276**, 93–96, https://doi.org/10.1126/science.276.5309.93.

Pöppelmeier, F., P. Blaser, M. Gutjahr, S. L. Jaccard, M. Frank, L. Max, and J. Lippold, 2020: Northern-sourced water dominated the Atlantic Ocean during the Last Glacial Maximum. *Geology*, **48**, 826–829, https://doi.org/10.1130/G47628.1.

Rackow, T., D. V. Sein, T. Semmler, S. Danilov, N. V. Koldunov, D. Sidorenko, Q. Wang, and T. Jung, 2019: Sensitivity of deep ocean biases to horizontal resolution in prototype CMIP6 simulations with AWI-CM1.0. *Geosci. Model Dev.*, **12**, 2635–2656, https://doi.org/10.5194/gmd-12-2635-2019.

Roberts, N. L., A. M. Piotrowski, J. F. McManus, and L. D. Keigwin, 2010: Synchronous deglacial overturning and water mass source changes. *Science*, **327**, 75–78, https://doi.org/10.1126/science.1178068.

Saenko, O. A., A. J. Weaver, and J. M. Gregory, 2003: On the link between the two modes of the ocean thermohaline circulation and the formation of global-scale water masses. *J. Climate*, **16**, 2797–2801, https://doi.org/10.1175/1520-0442(2003)016<2797:OTLBTT>2.0.CO;2.

Sarmiento, J. L., and J. R. Toggweiler, 1984: A new model for the role of the oceans in determining atmospheric pCO_2. *Nature*, **308**, 621–624, https://doi.org/10.1038/308621a0.

Schmidt, G. A., and Coauthors, 2014: Configuration and assessment of the GISS ModelE2 contributions to the CMIP5 archive. *J. Adv. Model. Earth Syst.*, **6**, 141–184, https://doi.org/10.1002/2013MS000265.

Schmittner, A., J. Green, and S.-B. Wilmes, 2015: Glacial ocean overturning intensified by tidal mixing in a global circulation model. *Geophys. Res. Lett.*, **42**, 4014–4022, https://doi.org/10.1002/2015GL063561.

——, and Coauthors, 2017: Calibration of the carbon isotope composition ($\delta^{13}C$) of benthic foraminifera. *Paleoceanogr. Paleoclimatol.*, **32**, 512–530, https://doi.org/10.1002/2016PA003072.

Sherriff-Tadano, S., A. Abe-Ouchi, M. Yoshimori, A. Oka, and W.-L. Chan, 2018: Influence of glacial ice sheets on the Atlantic meridional overturning circulation through surface wind change. *Climate Dyn.*, **50**, 2881–2903, https://doi.org/10.1007/s00382-017-3780-0.

Siddall, M., S. Khatiwala, T. van de Flierdt, K. Jones, S. L. Goldstein, S. R. Hemming, and R. F. Anderson, 2008: Towards explaining the Nd paradox using reversible scavenging in an ocean general circulation model. *Earth Planet. Sci. Lett.*, **274**, 448–461, https://doi.org/10.1016/j.epsl.2008.07.044.

Siegenthaler, U., and T. Wenk, 1984: Rapid atmospheric CO_2 variations and ocean circulation. *Nature*, **308**, 624–626, https://doi.org/10.1038/308624a0.

Sigman, D. M., and E. A. Boyle, 2000: Glacial/interglacial variations in atmospheric carbon dioxide. *Nature*, **407**, 859–869, https://doi.org/10.1038/35038000.

——, M. P. Hain, and G. H. Haug, 2010: The polar ocean and glacial cycles in atmospheric CO_2 concentration. *Nature*, **466**, 47–55, https://doi.org/10.1038/nature09149.

——, and Coauthors, 2020: The Southern Ocean during the ice ages: A review of the Antarctic surface isolation hypothesis, with comparison to the North Pacific. *Quat. Sci. Rev.*, **354**, 106732, https://doi.org/10.1016/j.quascirev.2020.106732.

Skinner, L. C., S. Fallon, C. Waelbroeck, E. Michel, and S. Barker, 2010: Ventilation of the deep Southern Ocean and deglacial CO_2 rise. *Science*, **328**, 1147–1151, https://doi.org/10.1126/science.1183627.

——, and Coauthors, 2017: Radiocarbon constraints on the glacial ocean circulation and its impact on atmospheric CO_2. *Nat. Commun.*, **8**, 16010, https://doi.org/10.1038/ncomms16010.

Speer, K., S. R. Rintoul, and B. Sloyan, 2000: The diabatic Deacon cell. *J. Phys. Oceanogr.*, **30**, 3212–3222, https://doi.org/10.1175/1520-0485(2000)030<3212:TDDC>2.0.CO;2.

St. Laurent, L., H. Simmons, and S. Jayne, 2002: Estimating tidally driven mixing in the deep ocean. *Geophys. Res. Lett.*, **29**, 2106, https://doi.org/10.1029/2002GL015633.

Stuiver, M., P. D. Quay, and H. G. Ostlund, 1983: Abyssal water carbon-14 distribution and the age of the world oceans. *Science*, **219**, 849–851, https://doi.org/10.1126/science.219.4586.849.

Stuut, J.-B. W., M. A. Prins, R. R. Schneider, G. J. Weltje, J. F. Jansen, and G. Postma, 2002: A 300-kyr record of aridity and wind strength in southwestern Africa: Inferences from grain-size distributions of sediments on Walvis Ridge, SE

Atlantic. *Mar. Geol.*, **180**, 221–233, https://doi.org/10.1016/S0025-3227(01)00215-8.

Sun, S., I. Eisenman, and A. L. Stewart, 2018: Does Southern Ocean surface forcing shape the global ocean overturning circulation? *Geophys. Res. Lett.*, **45**, 2413–2423, https://doi.org/10.1002/2017GL076437.

——, ——, L. Zanna, and A. L. Stewart, 2020: Surface constraints on the depth of the Atlantic meridional overturning circulation: Southern Ocean versus North Atlantic. *J. Climate*, **33**, 3125–3149, https://doi.org/10.1175/JCLI-D-19-0546.1.

Tagliabue, A., and Coauthors, 2009: Quantifying the roles of ocean circulation and biogeochemistry in governing ocean carbon-13 and atmospheric carbon dioxide at the last glacial maximum. *Climate Past*, **5**, 695–706, https://doi.org/10.5194/cp-5-695-2009.

Talley, L. D., 2003: Shallow, intermediate, and deep overturning components of the global heat budget. *J. Phys. Oceanogr.*, **33**, 530–560, https://doi.org/10.1175/1520-0485(2003)033<0530:SIADOC>2.0.CO;2.

——, 2013: Closure of the global overturning circulation through the Indian, Pacific, and Southern Oceans: Schematics and transports. *Oceanography*, **26**, 80–97, https://doi.org/10.5670/oceanog.2013.07.

Tamsitt, V., and Coauthors, 2017: Spiraling pathways of global deep waters to the surface of the Southern Ocean. *Nat. Commun.*, **8**, 172, https://doi.org/10.1038/s41467-017-00197-0.

——, R. P. Abernathey, M. R. Mazloff, J. Wang, and L. D. Talley, 2018: Transformation of deep water masses along Lagrangian upwelling pathways in the Southern Ocean. *J. Geophys. Res. Oceans*, **123**, 1994–2017, https://doi.org/10.1002/2017JC013409.

Toggweiler, J. R., 1999: Variation of atmospheric CO_2 by ventilation of the ocean's deepest water. *Paleoceanogr. Paleoclimatol.*, **14**, 571–588, https://doi.org/10.1029/1999PA900033.

van de Flierdt, T., A. M. Griffiths, M. Lambelet, S. H. Little, T. Stichel, and D. J. Wilson, 2016: Neodymium in the oceans: A global database, a regional comparison and implications for palaeoceanographic research. *Philos. Trans. Roy. Soc.*, **A374**, 20150293, https://doi.org/10.1098/rsta.2015.0293.

Waterhouse, A. F., and Coauthors, 2014: Global patterns of diapycnal mixing from measurements of the turbulent dissipation rate. *J. Phys. Oceanogr.*, **44**, 1854–1872, https://doi.org/10.1175/JPO-D-13-0104.1.

Watson, A. J., and A. C. Naveira Garabato, 2006: The role of Southern Ocean mixing and upwelling in glacial–interglacial atmospheric CO_2 change. *Tellus*, **58B**, 73–87, https://doi.org/10.1111/j.1600-0889.2005.00167.x.

——, G. K. Vallis, and M. Nikurashin, 2015: Southern Ocean buoyancy forcing of ocean ventilation and glacial atmospheric CO_2. *Nature*, **8**, 861–864, https://doi.org/10.1038/ngeo2538.

Weber, S. L., and Coauthors, 2007: The modern and glacial overturning circulation in the Atlantic Ocean in PMIP coupled model simulations. *Climate Past*, **3**, 51–64, https://doi.org/10.5194/cp-3-51-2007.

Wilmes, S.-B., A. Schmittner, and J. M. Green, 2019: Glacial ice sheet extent effects on modeled tidal mixing and the global overturning circulation. *Paleoceanogr. Paleoclimatol.*, **34**, 1437–1454, https://doi.org/10.1029/2019PA003644.

——, J. Green, and A. Schmittner, 2021: Enhanced vertical mixing in the glacial ocean inferred from sedimentary carbon isotopes. *Commun. Earth Environ.*, **2**, 166, https://doi.org/10.1038/s43247-021-00239-y.

Young, W. R., 2012: An exact thickness-weighted average formulation of the Boussinesq equations. *J. Phys. Oceanogr.*, **42**, 692–707, https://doi.org/10.1175/JPO-D-11-0102.1.

Zanna, L., S. Khatiwala, J. M. Gregory, J. Ison, and P. Heimbach, 2019: Global reconstruction of historical ocean heat storage and transport. *Proc. Natl. Acad. Sci. USA*, **116**, 1126–1131, https://doi.org/10.1073/pnas.1808838115.

Zhao, N., D. W. Oppo, K.-F. Huang, J. N. Howe, J. Blusztajn, and L. D. Keigwin, 2019: Glacial–interglacial Nd isotope variability of North Atlantic Deep Water modulated by North American ice sheet. *Nat. Commun.*, **10**, 5773, https://doi.org/10.1038/s41467-019-13707-z.